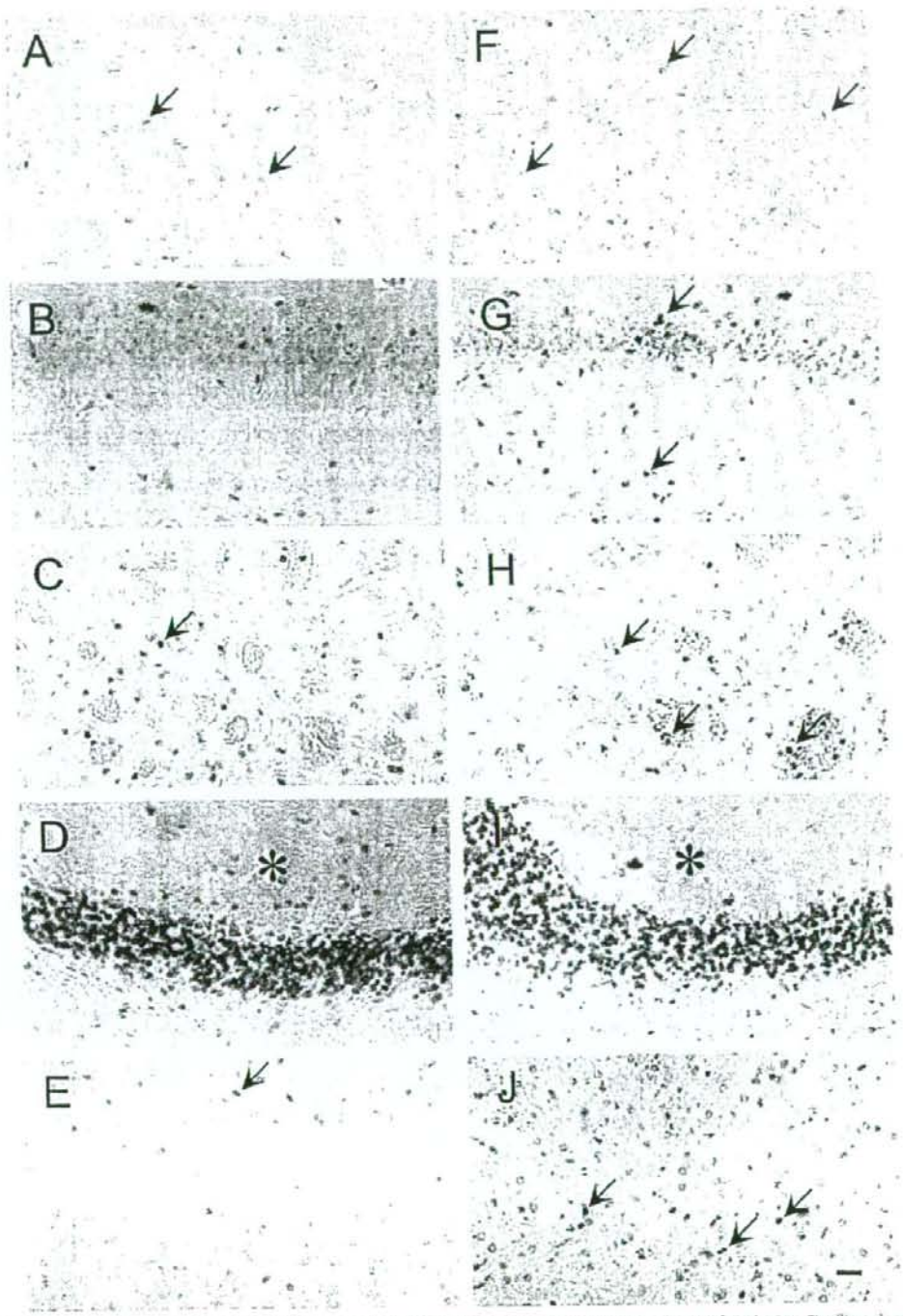

Figure 2. Immunohistochemical staining of citrullinated proteins in brain sections from control and ME7 scrapie-infected mice. Citrullinated proteins were detected in the brains of control (**A–E**) and scrapie-infected (**F–J**) mice at 160 days after inoculation. In the scrapie brain, citrullinated proteins (**arrows**) were more frequent than in control brains: cerebral cortex (**F**), hippocampus (**G**), striatum (**H**), cerebellum (**I**), and brain stem (**J**). **Asterisks** indicate the position of cerebellar molecular layer. Scale bar = 20 μm.

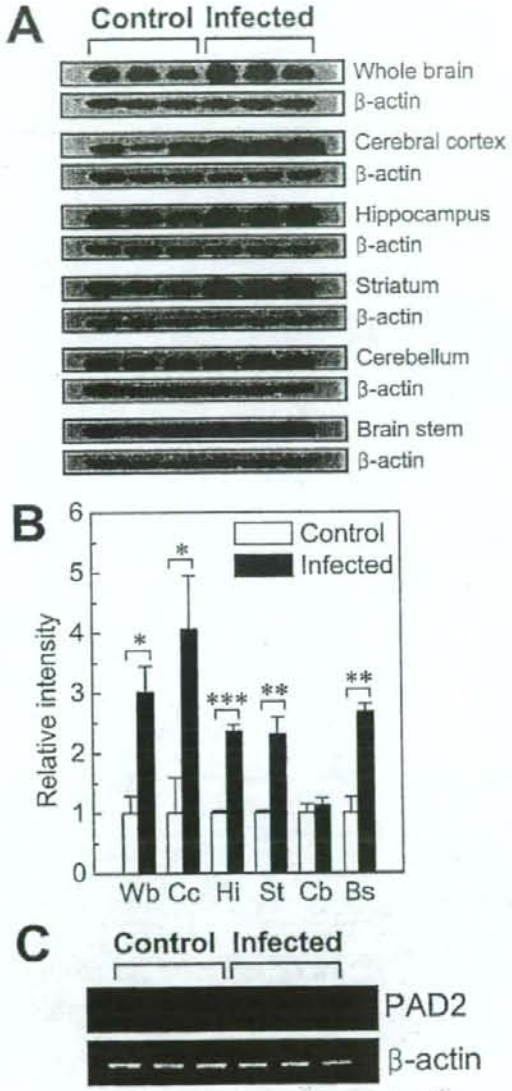

Figure 3. Comparison of expression level of PAD2 in brains from control and ME7 scrapie-infected mice. A: Expression level of PAD2 protein in whole brain and various brain sections of control and ME7-infected mice were analyzed by Western blot using a monoclonal anti-PAD2 antibody. Each lane shows the results for a homogenate obtained from dissected brain of each individual mouse. B: Densitometric analysis of bands in A normalized with β-actin. Wb, whole brain; Cc, cerebral cortex; Hi, hippocampus; St, striatum; Cb, cerebellum; Bs, brain stem. C: In whole brains, mRNA levels of PAD2 were analyzed by RT-PCR using three individuals of each group. Error bars represent SEM. $^{*}P < 0.05$, $^{**}P < 0.01$, $^{***}P < 0.001$.

mRNA in the whole brain of ME7 scrapie-infected mice compared to levels in controls. This result suggests that up-regulated expression of PAD2 protein seen in most brain regions is caused by an increase of gene expression in scrapie-infected mice.

Increased Immunofluorescence Staining of PAD2 in Reactive Astrocytes in Brains of Scrapie-Infected Mice

Next, to confirm the increased PAD2 expression and to determine the cellular localization of PAD2, immunohistochemical analysis was performed using various brain sections from control and scrapie-infected mice (Figure 4, A–E and F–J, respectively). In scrapie-infected brains, PAD2 immunoreactivity was more intense compared to control brains and these results correlated with the expression patterns of PAD2 protein in results of Western blot analysis (Figure 3A). According to previous reports, PAD2 is mainly expressed in glial cells such as astrocytes, oligodendrocytes, and microglial cells.[10–12] To further characterize the subcellular localization of PAD2, we performed double-immunofluorescence staining using GFAP, MBP, NeuN, and B4-isolectin as a marker for astrocytes, oligodendrocytes, neurons, and microglia, respectively. Interestingly, immunoreactivity was mainly observed in activated astrocytes in the brains of scrapie-infected mice. As can be seen in Figure 5, PAD2 was mainly co-localized with GFAP-positive astrocytes and in a few B4-isolectin-positive microglia, but not with MBP or NeuN. These data suggest that up-regulation of PAD2 expression in reactive astrocytes is responsible for the increased citrullinated proteins in the brains of scrapie-infected mice.

Elevated PAD2 Enzyme Activity in the Brains of Scrapie-Infected Mice

To investigate whether the increase in citrullinated proteins is attributable to higher levels of PAD2 enzyme activity and whether the increased PAD2 expression is correlated with its enzyme activity in scrapie-infected mice, we analyzed PAD2 enzyme activity in the brain homogenates of various sections from both control and ME7 scrapie-infected mice using benzoyl-L-arginine ethyl ester as a substrate as previously described.[9] PAD2 enzyme activity was significantly increased approximately twofold in whole brains as well as in hippocampus, striatum, and brain stem of scrapie-infected brains compared to controls (Figure 6A): whole brain [2.41-fold, control: 0.322 ± 0.052 (mean ± SEM, units); infected: 0.776 ± 0.039], hippocampus (2.19-fold, control: 0.342 ± 0.081; infected: 0.748 ± 0.120), striatum (2.48-fold, control: 0.256 ± 0.009; infected: 0.636 ± 0.082), and brain stem (1.99-fold, control: 0.589 ± 0.028; infected: 1.172 ± 0.055). The difference from controls was not significant in cerebral cortex (control: 0.193 ± 0.022; infected: 0.294 ± 0.032) or in cerebellum (control: 0.312 ± 0.041; infected: 0.419 ± 0.035). To determine whether the amount of PAD2 protein is associated with changes in enzyme activity, we compared the expression level of PAD2 protein in 50 μg of total protein from whole brain and from different brain regions of control and scrapie-infected mice. As shown in Figure 6B, the expression levels of PAD2 protein in cerebral cortex and in cerebellum were lower than other regions but still higher

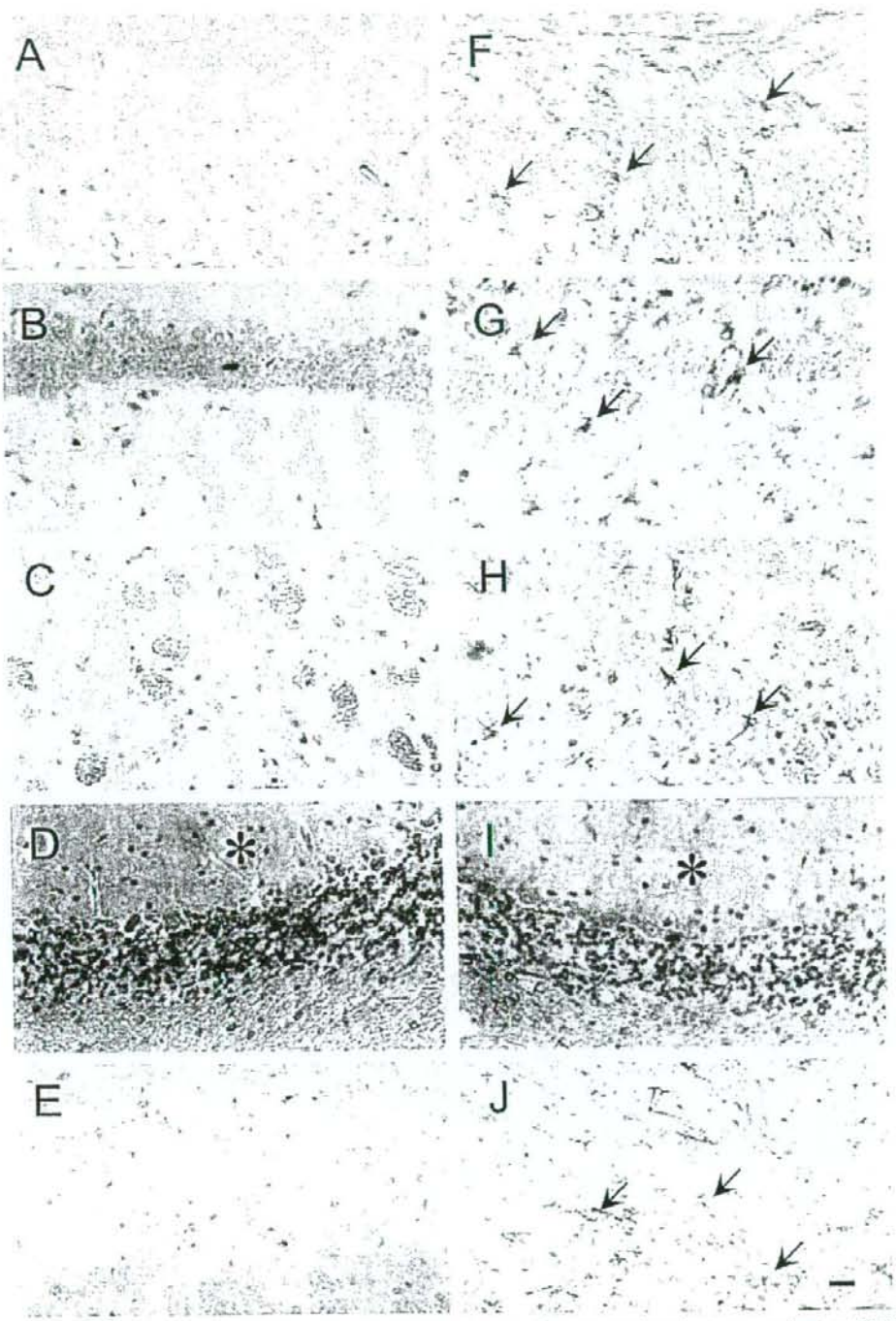

Figure 4. Expression of PAD2 in various brain sections. Immunohistochemical staining of PAD2 was performed using a monoclonal anti-PAD2 antibody in various brain sections from control (**A–E**) and ME7 scrapie-infected (**F–J**) mice. PAD2 was observed in dissected control and scrapie-infected brains at 160 days after inoculation with the ME7 scrapie strain. PAD2-positive cells were strongly immunostained in scrapie-infected brains and its immunoreactivity was observed in reactive astrocytes (**arrows**). **A** and **F**: Cerebral cortex; **B** and **G**: hippocampus; **C** and **H**: striatum; **D** and **I**: cerebellum; **E** and **J**: brain stem. **Asterisks** indicate the position of cerebellar molecular layer. Scale bar = 20 μm.

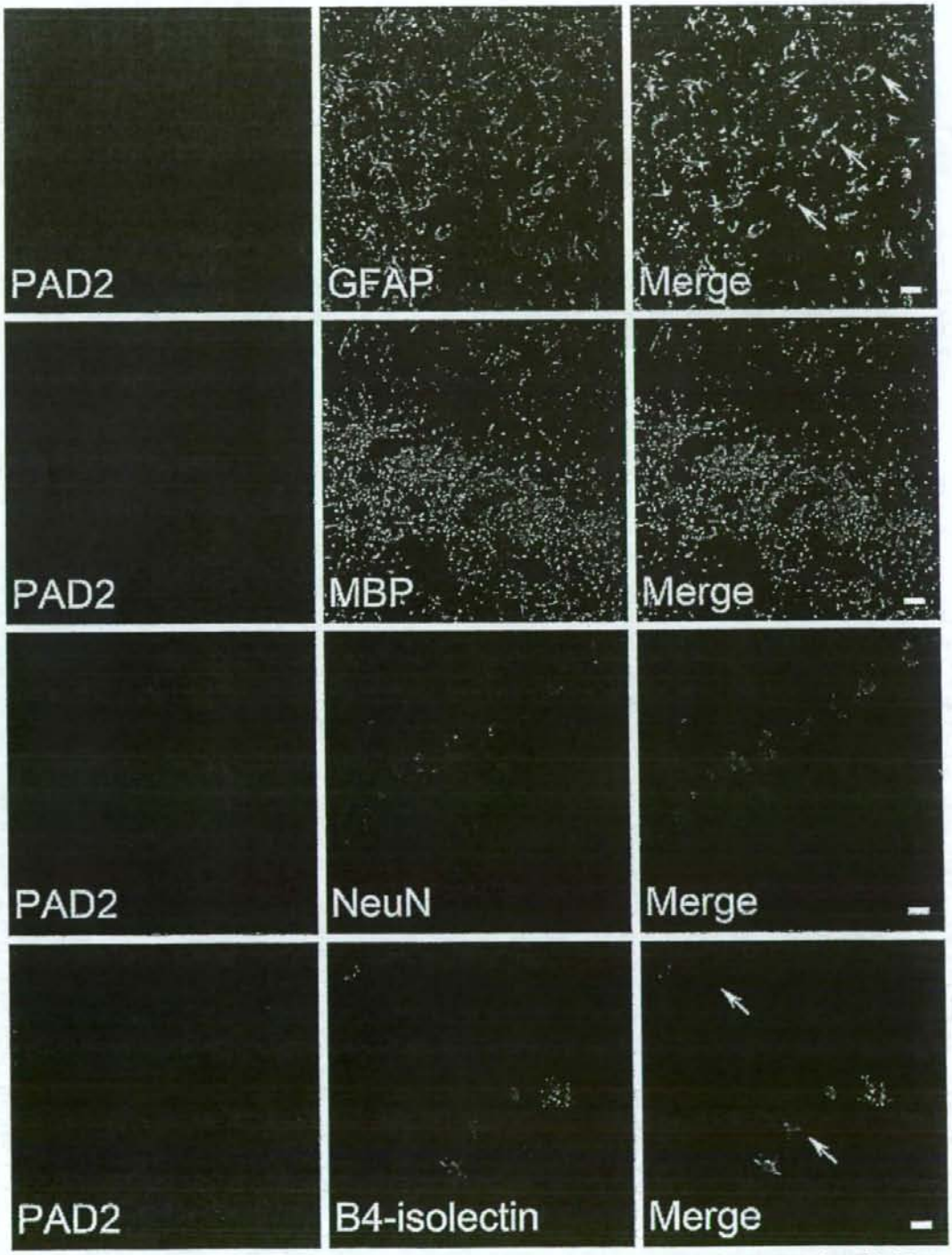

Figure 5. Cellular localization of PAD2 in scrapie-infected brains. The brain sections were doubly immunostained with anti-PAD2 and one of the following antibodies: astrocyte-specific GFAP, oligodendrocyte-specific MBP, neuron-specific NeuN, or microglia-specific B4-isolectin antibodies. Slides were examined under confocal laser-scanning microscopy. Note that PAD2-positive cells were strongly co-localized in cells positive for GFAP (**arrows**) with very few B4-isolectin-positive microglia (**arrows**). Scale bars = 20 μm.

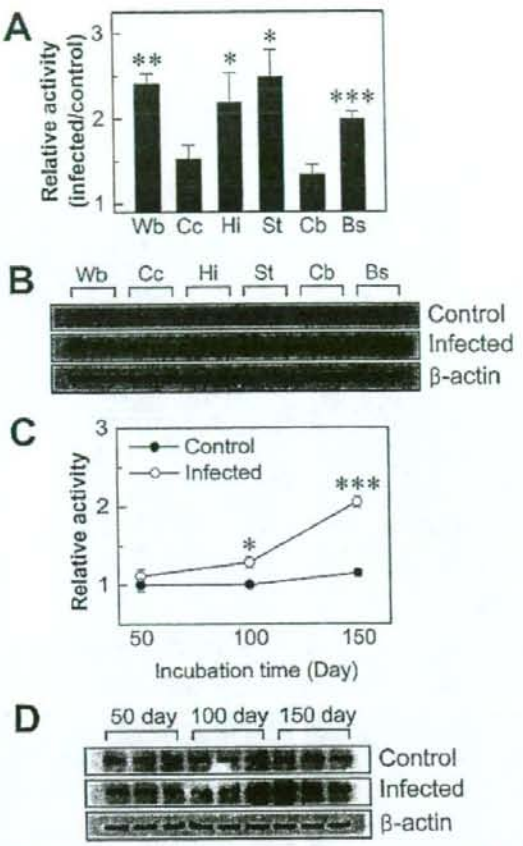

Figure 6. Measurement of PAD2 enzyme activity in mouse brains. **A:** PAD2 enzyme activity in the brains of control and ME7-infected mice. PAD2 enzyme activity was determined as described in the Materials and Methods. The results are presented as a column graph of values in infected samples relative to controls. Values are mean ± SEM obtained from separate assays of three mouse brains ($n = 3$). **B:** Comparison of the expression levels of PAD2 protein in various brain sections of scrapie-infected mice. Wb, whole brain; Cc, cerebral cortex; Hi, hippocampus; St, striatum; Cb, cerebellum; Bs, brain stem. **C:** PAD2 enzyme activity was determined at different time points during scrapie incubation period using the whole brains of control (**filled circle**) and ME7-infected mice (**open circle**) as indicated ($n = 3$). **D:** Expression level of PAD2 protein in whole brains of control and scrapie-infected mice at 50, 100, and 150 days after inoculation was analyzed by Western blotting. Each experiment was repeated at least three times, and similar results were obtained. $^{*}P < 0.05$, $^{**}P < 0.01$, $^{***}P < 0.001$.

than controls. It should be noted that all regions showed increased levels of citrullinated proteins in scrapie-infected brains compared to controls (Figures 1 and 2). The results suggest that demonstration of PAD2 enzyme activity (Figure 6A) may require a certain amount of PAD2 protein to see the difference of enzyme activity and its citrullination between control and scrapie-infected brains in our *in vitro* assay. In addition, to determine whether the enzyme activity and protein expression of PAD2 are correlated with the progress of this disease, we also examined PAD2 enzyme activity and its protein expression at different time points during scrapie incubation period using whole brains of scrapie-infected and control mice (Figure 6, C and D). In Figure 6C, no difference between scrapie-infected and control brains was observed at 50 days after inoculation. However, the PAD2 enzyme activity tended to increase relative to the stage of scrapie development and was significantly increased at 100 and 150 days after inoculation; this time corresponds to marked accumulation of PAD2 (Figure 6D) and citrullinated proteins (data not shown). These results suggest that increased PAD activity and its protein expression might be responsible for the increased citrullinated proteins at end stage of scrapie infection.

Identification of Citrullinated Proteins by 2-DE and MALDI-TOF Mass Spectrometry

For identification of various citrullinated proteins in scrapie-infected brains, we performed 2-DE analysis using whole brains as well as three different brain regions: hippocampus, cerebellum, and brain stem. We chose these three regions because i) hippocampus is the most damaged brain region, ii) cerebellum showed a marked increase in citrullinated bands between 100 kDa and 150 kDa, and iii) brain stem has shown the highest expression of PAD2 after infection with the ME7 scrapie strain. Figure 7 shows representative 2-DE gels for the whole brain from control and ME7 scrapie-infected mice. The rectangular areas (Figure 7, a–c) in 2-DE gels were representative immunoblotting for the whole brain (Figure 7a′), cerebellum (Figure 7b′), and brain stem (Figure 7c′). Using an antibody to modified citrulline, we detected numerous citrullinated spots in dissected brain regions of scrapie-infected brains that were not seen in controls (Figure 7, a′–c′; right). In case of hippocampus, citrullinated spots detected were the same as those seen in whole brain and brain stem (data not shown).

To identify the citrullinated spots, we analyzed peptide spots by MALDI-TOF mass spectrometer. Identified citrullinated proteins in the brains of scrapie-infected mice are summarized in Table 1. We have found some known citrullinated proteins including GFAP and MBP as well as new substrates for PAD2 including neuron-specific enolase (NSE; 2-phospho-D-glycerate hydrolase), fructose 1,6-bisphosphate aldolase A and C (ALDC), and mitochondrial malate dehydrogenase 2 (MDH2), and voltage-dependent anion channel 1 (VDAC1).

Expression Levels of Identified Citrullinated Proteins; Aldolase C, Neuron-Specific Enolase, MBP, and GFAP

Based on the result of MALDI-TOF analysis, we performed Western blot analysis to determine the expression pattern of identified citrullinated proteins in control and scrapie-infected brains. As shown in Figure 8, interestingly, ALDC, a newly identified citrullinated protein in this study was significantly increased in scrapie-infected brains compared to controls. It has been known that ALDC is mainly expressed in astrocytes and Purkinje cells.[23,24] In immunohistochemical staining of ALDC in

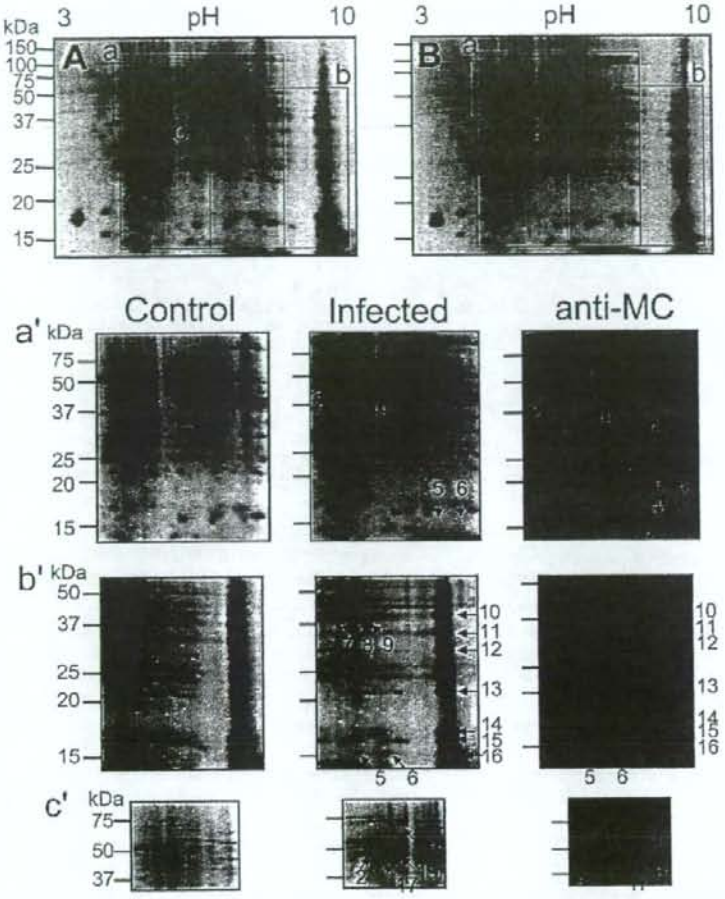

Figure 7. Detection of citrullinated proteins from two-dimensional electrophoresis. The 2-DE gels show CBBG-250 staining of proteins from brains of control and infected mice (**A** and **B**, respectively). The rectangular areas (**a**–**c**) of the 2-DE gels represent a part of the 2-DE gels in each region of control and infected brains (**left** and **middle**, respectively) and citrullinated proteins (anti-MC) assayed by Western blot (**right**) from whole brain (**a'**), cerebellum (**b'**), brain stem (**c'**). Serial numbers in each infected region were used to distinguish between the identified citrullinated proteins in each region. The second spot in whole brain was the same as the one in brain stem, the fifth and sixth spots in whole brain were equal to the spots in cerebellum. The 19th spot was also detected in hippocampus (data not shown). Each experiment was repeated at least three times, and similar results were obtained.

the brains of control and infected mice, we also observed highly intense staining of ALDC, mainly in astrocytes of hippocampus (data not shown). The results for NSE showed slightly decreased levels in hippocampus (37%) and cerebellum (17%) of scrapie brain compared to controls, whereas the quantities in other brain regions appeared to be very similar in infected and controls (Figure 8). Strikingly, MBP was decreased in scrapie-positive mice compared to control animals in several regions, including cerebral cortex, hippocampus, striatum, and brain stem; the difference from control was quite marked in hippocampus and striatum. In accordance with previous reports, GFAP was increased in all infected brain regions that reflects the pathological finding of astrocytosis.

Discussion

It has been postulated that citrullination of proteins has important effects on their structure and functions. Citrullination, an irreversible posttranslational modification, has been associated with the pathogenesis of several neurodegenerative diseases including AD and MS.[15,17] Citrullinated proteins in these diseases are thought to play a role during disease initiation and/or disease progression. The mouse models of neurodegenerative diseases provide a rapid and inexpensive means of studying pathogenesis and pathology of human diseases.

In the present study, we demonstrated for the first time that protein citrullination occurs in a widely used model of prion diseases, ie, ME7 scrapie-infected mice. PAD enzymes have been shown to increase in various abnormal conditions *in vivo* including transgenic animal models of demyelinating diseases,[25] optic nerve damage in glaucoma,[26] and in hippocampi of AD patients.[15] However, the regulatory mechanism of PAD2 expression and of the induction of citrullinated proteins involved in the pathogenesis of various diseases has not been clarified. Using a model system of scrapie-infected mice provides a number of advantages in that scrapie strains have specific parameters of incubation period, location of histopathological changes, and mouse strain susceptibility. There-

Table 1. Summary of identified citrullinated proteins in ME7 scrapie-infected mice

Spot No.	Identification	Sequence coverage (%)	pI	kDa	NCBI accession no.	*Z-value
1	Tubulin, beta 2	24	4.8	50.29	NP_033476	2.07
2	Enolase 2, neuron-specific	40	5.0	47.62	NP_038537	2.37
3	Glial fibrillary acidic protein	50	5.0	46.57	AAK56090	2.15
4	Enolase 1, alpha	42	6.4	47.47	P17182	2.33
5	Myelin basic protein	36	11.8	14.19	AAA39497	1.68
6	Myelin basic protein	56	11.8	14.19	AAA39497	1.69
7	Aldolase 3, C isoform	36	6.7	38.78	P05063	2.41
8	Aldolase 3, C isoform	39	6.7	38.78	P05063	2.39
9	Aldolase 3, C isoform	35	6.7	38.78	P05063	2.24
10	Aldolase 1, A isoform	45	8.8	39.79	NP_031464	2.40
11	Malate dehydrogenase 2	54	9.4	36.05	NP_032643	2.37
12	Voltage-dependent anion channel 1	36	8.7	32.50	Q60932	2.29
13	Peroxiredoxin 1	39	8.6	22.39	NP_035164	2.08
14	Cofilin 1	51	8.5	18.77	NP_031713	2.33
15	Peptidylprolyl isomerase A	36	7.9	18.12	NP_032933	1.80
16	Myelin basic protein	61	11.8	14.19	AAA39497	2.41
17	Glial fibrillary acidic protein	41	5.0	46.57	AAK56090	1.53
18	Heat shock protein 8	28	5.3	71.08	AAH66191	2.38
19	Glial fibrillary acidic protein	28	5.0	46.57	AAK56090	2.38

Citrullinated spots were identified from spots 1–6 in whole brain, spots 7–16 in cerebellum, and spots 17–19 in brain stem. The 19th spot was also identified in hippocampus from ME7 scrapie-infected mice. *Z-value and its corresponding confidence are following: 1.282, 90.0%; 1.645, 95.0%; 2.326, 99.0%; 3.090, 99.9%.

fore, the combination of scrapie strain-mouse strain may give an area-specific difference in the expression pattern of PAD2 and hypercitrullinated proteins that can be correlated with histopathological changes in each brain region. The situation is more complex with human disease because of different or even unknown causes and the inability to assess brain changes during the course of the disease. However, studies with the mouse models of scrapie can provide a basis for studying citrullination in postmortem tissue from a variety of diseases.

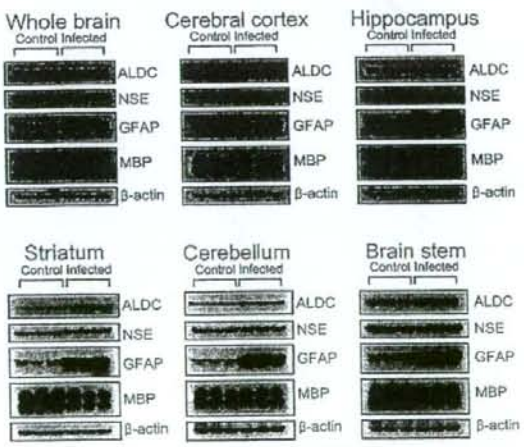

Figure 8. Expression levels of several identified citrullinated proteins in brains of control and scrapie-infected mice. Proteins that had been identified as citrullinated were analyzed by Western blot in homogenates from whole brain, cerebral cortex, hippocampus, striatum, cerebellum, and brain stem. The proteins included ALDC, NSE, GFAP, MBP, and actin as a control stain. Note that ALDC and GFAP were significantly increased in scrapie-infected mice. In contrast, NSE was slightly decreased in whole brain, hippocampus, and cerebellum and MBP was significantly decreased in cerebral cortex, brain stem, hippocampus, and striatum in brains from scrapie-infected mice compared to controls.

An important aspect of citrullination *in vivo* and *in vitro* is that PAD enzymes require ~100-fold higher than the normal intracellular Ca^{2+} level for its activation.[7] PrP^{Sc} is associated with elevation of intracellular Ca^{2+} released from endoplasmic reticulum in neuroblastoma cells.[27] PrP 106-126 peptide that shares several characteristics with PrP^{Sc} induces Ca^{2+} release from endoplasmic reticulum and mitochondria.[28,29] These reports suggest that intracellular Ca^{2+} is increased in a variety of cells in the brains of scrapie-infected mice. The increase in intracellular Ca^{2+} during scrapie infection would augment the activity of PAD2, which, in turn, would lead to citrullination of various proteins. In addition, malfunctioning of some of these citrullinated proteins could play a role in the pathogenesis of the pathological changes that are seen in prion diseases. This scenario is supported by our findings of increased PAD2 and citrullinated proteins combined with the above-noted reports on the relationship between Ca^{2+} metabolism and scrapie.

Because the current knowledge of the molecular features of PAD enzymes is limited, it is still unclear whether activation of PAD2 is a cause of or an effect of the progression of prion diseases. In a previous article, PAD2 was increased and accumulated in the hippocampus during the progress of AD.[15] This finding suggests that because PAD2 was increased even during early stages of AD, PAD2 activation may be related to onset of neurodegenerative change in this disease. It has been suggested that the activation of PADs is induced by elevation of intracellular calcium levels or leakage of the enzyme to the extracellular space as a result of cell membrane disruption.[30,31] Although the increased intracellular calcium levels appear to be the major regulator of PADs, it has been shown that some hormones, including estrogen, progesterone, and insulin, and other molecules that induce differentiation of cells regulate the activity of PAD2 and other PAD isotypes.[32] Moreover, PAD2 activity is

enhanced in a reducing environment,[33,34] indicating that PAD activity can be up-regulated by modulation of disulfide bonds. Thus, these data show that the regulation of PAD2 activity is highly complex with multiple interlocking control points.

Results of Western blot analysis using an antibody to citrullinated proteins have shown a variety of strong bands between 10 kDa to 150 kDa. A number of these were markedly increased in scrapie compared to control brain regions. We analyzed homogenates of whole brain, brain stem, and cerebellum from control and scrapie-infected mice by 2-DE and MALDI-TOF mass spectrometry analyses that yielded 13 distinct citrullinated proteins (Table 1). We could not establish the identity of the bands in brain stem and cerebellum between 100 kDa to 150 kDa using 2-DE. Three distinct citrullinated proteins were previously demonstrated: GFAP in AD,[15] MBP in MS,[35] and α-enolase in rheumatoid arthritis (RA).[36] These proteins relate to energy production pathway and to cellular structure.

GFAP and MBP are well known to show increases in citrullination in degenerative disorders. In ME7-infected mice, there were pronounced increases in the levels of citrullinated GFAP compared to controls in all brain regions tested (Figure 1). Citrullinated spots were seen at 50 kDa and at 15 kDa, which are the molecular weight designations for GFAP and MBP, respectively. GFAP and MBP are arginine-rich proteins that have 47 arginine residues in GFAP and 19 residues in MBP, in both human and mouse. Any arginine residue can be citrullinated, and a number of specific rules of citrullination have been formulated.[8] The expression level of GFAP was increased in every brain region tested; in contrast, there was a marked decrease in MBP in all regions except cerebellum (Figure 8). These results may reflect the unfolding of citrullinated MBP and subsequent rapid degradation by cathepsin D,[37] an enzyme that is increased in scrapie.[38] A decrease of MBP may evoke demyelinating changes in prion diseases.[39,40] In scrapie-infected mice, there is decreased expression of MBP, but the MBP present is citrullinated abundantly (Figures 1 and 8 and Table 1). A high proportion of GFAP-positive cells contain citrullinated proteins, although there are cells that appear to be negative for staining. NSE and MBP were also shown to be positive for citrullination, indicating that neurons and oligodendrocytes are also affected. Neurons could also be affected indirectly in that citrullination of proteins in astrocytes could affect their role in physiological support of neurons; this, in turn, could lead to neuron degeneration and loss.

Interestingly, we found that energy regulation-related proteins such as enolases, aldolases, MDH2, and VDAC1 can be citrullinated by PAD2 in scrapie. α-Enolase, a glycolytic enzyme, has been identified as an autoantigen in diseases such as MS[41] and Hashimoto's encephalopathy.[42] NSE has been used as a pathogenic marker in various neurological diseases including MS,[43] acute ischemic stroke,[44] and RA.[36,45] In addition, previous reports showed an early elevation of NSE in cerebrospinal fluid of Creutzfeldt-Jakob disease (CJD) patients, which decreased with disease duration, and this early elevation is considered to support the diagnosis of CJD.[46–48] We also examined the expression level of NSE in brains of scrapie-infected mice and the results showed slightly decreased levels in hippocampus and cerebellum of scrapie brain compared to controls; levels in other brain regions were similar in control and scrapie (Figure 8).

Aldolase A is suggested as a candidate autoantigen in RA[45] and in AD,[49] and its deficiency is associated with a hemolytic anemia.[50] ALDC has been termed "scrapie-responsive protein 2 (scrg2)," and its mRNA is increased in scrapie infection.[51,52] We also confirmed an increase of ALDC in scrapie-infected mice using Western blot (Figure 8) and immunohistochemical analyses (data not shown). In addition, we are first to report that ALDC is a new candidate citrullinated protein and that it was mainly expressed in reactive astrocytes of scrapie-infected brain. Although ALDC is a predominant type in brain, the total aldolase activity was not significantly changed by scrapie infection (data not shown). It is possible that citrullination of ALDC leads to its accumulation, but generates its inactive form because there were no significant changes of enzyme activity. MDH2, an enzyme in the citric acid cycle, is thought to play a key role in the pathophysiology of schizophrenia.[53] However, thus far, the evidence of MDH2 involvement in disease is weak. VDAC1 is a mitochondrial membrane protein that plays a role in the transport of various metabolites across the outer mitochondrial membrane and that regulates mitochondrial Ca^{2+} homeostasis[54] and apoptosis in conjunction with the Bcl-2 family.[55] Previous reports have demonstrated that several divalent metal ions including Ca^{2+} are increased in mitochondrial membrane fractions of scrapie-infected mice.[56] Assuming that citrullination of VDAC affects its role in membrane permeability, this in turn could lead to changes in Ca^{2+} homeostasis and in the induction of neuronal cell death in prion diseases.

Finally, we have identified more candidate citrullinated proteins such as cofilin 1, peptidylprolyl isomerase A, and peroxiredoxin 1. Cofilin 1 is an actin-binding protein that modulates neuronal actin dynamics and synaptic plasticity.[57,58] Peptidylprolyl isomerase A has multiple roles in protein refolding, signal transduction, and cell cycle regulation.[59] Peroxiredoxin 1 is a thiol-specific multifunctional antioxidant enzyme whose major role is a defense against oxidative stress through peroxidase activity.[60] In a recent report, the expression of this gene was increased by ~30% in 139A scrapie-infected mice.[61] Further investigations are required to characterize these candidate citrullinated proteins and their physiological functions.

Herein we demonstrated the increased expression of PAD2 and identified a number of citrullinated proteins in the ME7-infected mouse model of prion diseases. Whether the citrullination of these proteins has physiological consequences remains unknown. Nevertheless, PAD2 may play a role in the onset and progression of prion diseases by abnormal disruption of Ca^{2+} homeostasis, and/or by increasing citrullinated proteins. Furthermore, citrullinated proteins may serve as a useful marker for human neurodegenerative diseases. The further study of these citrullinated proteins may provide

more definitive answers about molecular functions and pathological mechanisms in prion diseases, including human neurodegenerative disorders.

References

1. Prusiner SB: Prions. Proc Natl Acad Sci USA 1998, 95:13363–13383
2. Aguzzi A, Heikenwalder M, Polymenidou M: Insights into prion strains and neurotoxicity. Nat Rev Mol Cell Biol 2007, 8:552–561
3. Cronier S, Laude H, Peyrin JM: Prions can infect primary cultured neurons and astrocytes and promote neuronal cell death. Proc Natl Acad Sci USA 2004, 101:12271–12276
4. Wong K, Qiu Y, Hyun W, Nixon R, VanCleff J, Sanchez-Salazar J, Prusiner SB, DeArmond SJ: Decreased receptor-mediated calcium response in prion-infected cells correlates with decreased membrane fluidity and IP3 release. Neurology 1996, 47:741–750
5. Takenouchi T, Iwamaru Y, Imamura M, Kato N, Sugama S, Fujita M, Hashimoto M, Sato M, Okada H, Yokoyama T, Mohri S, Kitani H: Prion infection correlates with hypersensitivity of P2X7 nucleotide receptor in a mouse microglial cell line. FEBS Lett 2007, 581:3019–3026
6. Inagaki M, Takahara H, Nishi Y, Sugawara K, Sato C: Ca^{2+}-dependent deimination-induced disassembly of intermediate filaments involves specific modification of the amino-terminal head domain. J Biol Chem 1989, 264:18119–18127
7. Vossenaar ER, Zendman AJ, van Venrooij WJ, Pruijn GJ: PAD, a growing family of citrullinating enzymes: genes, features and involvement in disease. Bioessays 2003, 25:1106–1118
8. Tarcsa E, Marekov LN, Mei G, Melino G, Lee SC, Steinert PM: Protein unfolding by peptidylarginine deiminase. Substrate specificity and structural relationships of the natural substrates trichohyalin and filaggrin. J Biol Chem 1996, 271:30709–30716
9. Watanabe K, Akiyama K, Hikichi K, Ohtsuka R, Okuyama A, Senshu T: Combined biochemical and immunochemical comparison of peptidylarginine deiminases present in various tissues. Biochim Biophys Acta 1988, 966:375–383
10. Vincent SR, Leung E, Watanabe K: Immunohistochemical localization of peptidylarginine deiminase in the rat brain. J Chem Neuroanat 1992, 5:159–168
11. Asaga H, Senshu T: Combined biochemical and immunocytochemical analyses of postmortem protein deimination in the rat spinal cord. Cell Biol Int 1993, 17:525–532
12. Akiyama K, Sakurai Y, Asou H, Senshu T: Localization of peptidylarginine deiminase type II in a stage-specific immature oligodendrocyte from rat cerebral hemisphere. Neurosci Lett 1999, 274:53–55
13. Keilhoff G, Prell T, Langnaese K, Mawrin C, Simon M, Fansa H, Nicholas AP: Expression pattern of peptidylarginine deiminase in rat and human Schwann cells. Dev Neurobiol 2008, 68:101–114
14. Asaga H, Ishigami A: Protein deimination in the rat brain after kainate administration: citrulline-containing proteins as a novel marker of neurodegeneration. Neurosci Lett 2001, 299:5–8
15. Ishigami A, Ohsawa T, Hiratsuka M, Taguchi H, Kobayashi S, Saito Y, Murayama S, Asaga H, Toda T, Kimura N, Maruyama N: Abnormal accumulation of citrullinated proteins catalyzed by peptidylarginine deiminase in hippocampal extracts from patients with Alzheimer's disease. J Neurosci Res 2005, 80:120–128
16. Moscarello MA, Wood DD, Ackerley C, Boulias C: Myelin in multiple sclerosis is developmentally immature. J Clin Invest 1994, 94:146–154
17. Moscarello MA, Mastronardi FG, Wood DD: The role of citrullinated proteins suggests a novel mechanism in the pathogenesis of multiple sclerosis. Neurochem Res 2007, 32:251–256
18. Choi EK, Zaidi NF, Miller JS, Crowley AC, Merriam DE, Lilliehook C, Buxbaum JD, Wasco W: Calsenilin is a substrate for caspase-3 that preferentially interacts with the familial Alzheimer's disease-associated C-terminal fragment of presenilin 2. J Biol Chem 2001, 276:19197–19204
19. Senshu T, Sato T, Inoue T, Akiyama K, Asaga H: Detection of citrulline residues in deiminated proteins on polyvinylidene difluoride membrane. Anal Biochem 1992, 203:94–100
20. Rothnagel JA, Rogers GE: Citrulline in proteins from the enzymatic deimination of arginine residues. Methods Enzymol 1984, 107:624–631
21. Ishigami A, Ohsawa T, Asaga H, Akiyama K, Kuramoto M, Maruyama N: Human peptidylarginine deiminase type II: molecular cloning, gene organization, and expression in human skin. Arch Biochem Biophys 2002, 407:25–31
22. Toda T, Satoh M, Sugimoto M, Goto M, Furuichi Y, Kimura N: A comparative analysis of the proteins between the fibroblasts from Werner's syndrome patients and age-matched normal individuals using two-dimensional gel electrophoresis. Mech Ageing Dev 1998, 100:133–143
23. Kumanishi T, Watabe K, Washiyama K: An immunohistochemical study of aldolase C in normal and neoplastic nervous tissues. Acta Neuropathol (Berl) 1985, 67:309–314
24. Buono P, D'Armiento FP, Terzi G, Alfieri A, Salvatore F: Differential distribution of aldolase A and C in the human central nervous system. J Neurocytol 2001, 30:957–965
25. Moscarello MA, Pritzker L, Mastronardi FG, Wood DD: Peptidylarginine deiminase: a candidate factor in demyelinating disease. J Neurochem 2002, 81:335–343
26. Bhattacharya SK, Bhat MB, Takahara H: Modulation of peptidyl arginine deiminase 2 and implication for neurodegeneration. Curr Eye Res 2006, 31:1063–1071
27. Hetz C, Russelakis-Carneiro M, Maundrell K, Castilla J, Soto C: Caspase-12 and endoplasmic reticulum stress mediate neurotoxicity of pathological prion protein. EMBO J 2003, 22:5435–5445
28. O'Donovan CN, Tobin D, Cotter TG: Prion protein fragment PrP-(106-126) induces apoptosis via mitochondrial disruption in human neuronal SH-SY5Y cells. J Biol Chem 2001, 276:43516–43523
29. Ferreiro E, Resende R, Costa R, Oliveira CR, Pereira CM: An endoplasmic-reticulum-specific apoptotic pathway is involved in prion and amyloid-beta peptides neurotoxicity. Neurobiol Dis 2006, 23:669–678
30. Takahara H, Okamoto H, Sugawara K: Calcium-dependent properties of peptidylarginine deiminase from rabbit skeletal muscle. Agric Biol Chem 1986, 50:2899–2904
31. Nijenhuis S, Zendman AJ, Vossenaar ER, Pruijn GJ, vanVenrooij WJ: Autoantibodies to citrullinated proteins in rheumatoid arthritis: clinical performance and biochemical aspects of an RA-specific marker. Clin Chim Acta 2004, 350:17–34
32. Méchin MC, Sebbag M, Arnaud J, Nachat R, Foulquier C, Adoue V, Coudane F, Duplan H, Schmitt AM, Chavanas S, Guerrin M, Serre G, Simon M: Update on peptidylarginine deiminases and deimination in skin physiology and severe human diseases. Int J Cosmet Sci 2007, 29:147–168
33. Fujisaki M, Sugawara K: Properties of peptidylarginine deiminase from the epidermis of newborn rats. J Biochem (Tokyo) 1981, 89:257–263
34. Kubilus J, Baden HP: Purification and properties of a brain enzyme that deiminates proteins. Biochim Biophys Acta 1983, 745:285–291
35. Wood DD, Bilbao JM, O'Connors P, Moscarello MA: Acute multiple sclerosis (Marburg type) is associated with developmentally immature myelin basic protein. Ann Neurol 1996, 40:18–24
36. Kinloch A, Tatzer V, Wait R, Peston D, Lundberg K, Donatien P, Moyes D, Taylor PC, Venables PJ: Identification of citrullinated alpha-enolase as a candidate autoantigen in rheumatoid arthritis. Arthritis Res Ther 2005, 7:R1421–R1429
37. Pritzker LB, Joshi S, Gowan JJ, Harauz G, Moscarello MA: Deimination of myelin basic protein. 1. Effect of deimination of arginyl residues of myelin basic protein on its structure and susceptibility to digestion by cathepsin D. Biochemistry 2000, 39:5374–5381
38. Diedrich JF, Minnigan H, Carp RI, Whitaker JN, Race R, Frey II W, Haase AT: Neuropathological changes in scrapie and Alzheimer's disease are associated with increased expression of apolipoprotein E and cathepsin D in astrocytes. J Virol 1991, 65:4759–4768
39. Neufeld MY, Josiphov J, Korczyn AD: Demyelinating peripheral neuropathy in Creutzfeldt-Jakob disease. Muscle Nerve 1992, 15:1234–1239
40. Kovács T, Arányi Z, Szirmai I, Lantos PL: Creutzfeldt-Jakob disease with amyotrophy and demyelinating polyneuropathy. Arch Neurol 2002, 59:1811–1814
41. Almeras L, Lefranc D, Drobecq H, de Seze J, Dubucquoi S, Vermersch P, Prin L: New antigenic candidates in multiple sclerosis: identification by serological proteome analysis. Proteomics 2004, 4:2184–2194
42. Yoneda M, Fujii A, Ito A, Yokoyama H, Nakagawa H, Kuriyama M:

High prevalence of serum autoantibodies against the amino terminal of alpha-enolase in Hashimoto's encephalopathy. J Neuroimmunol 2007, 185:195–200
43. Forooghian F, Cheung RK, Smith WC, O'Connor P, Dosch HM: Enolase and arrestin are novel nonmyelin autoantigens in multiple sclerosis. J Clin Immunol 2007, 27:388–396
44. Anand N, Stead LG: Neuron-specific enolase as a marker for acute ischemic stroke: a systematic review. Cerebrovasc Dis 2005, 20:213–219
45. Ukaji F, Kitajima I, Kubo T, Shimizu C, Nakajima T, Maruyama I: Serum samples of patients with rheumatoid arthritis contain a specific autoantibody to "denatured" aldolase A in the osteoblast-like cell line MG-63. Ann Rheum Dis 1999, 58:169–174
46. Jimi T, Wakayama Y, Shibuya S, Nakata H, Tomaru T, Takahashi Y, Kosaka K, Asano T, Kato K: High levels of nervous system-specific proteins in cerebrospinal fluid in patients with early stage Creutzfeldt-Jakob disease. Clin Chim Acta 1992, 211:37–46
47. Evers S, Droste DW, Lüdemann, P, Oberwittler C: Early elevation of cerebrospinal fluid neuron-specific enolase of cerebrospinal fluid neuron-specific enolase in Creutzfeldt-Jakob disease. J Neurol 1998, 145:52–53
48. Kropp S, Zerr I, Schulz-Schaeffer WJ, Riedemann C, Bodemer M, Laske C, Kretzschmar HA, Poser S: Increase of neuron-specific enolase in patients with Creutzfeldt-Jakob disease. Neurosci Lett 1999, 261:124–126
49. Mor F, Izak M, Cohen IR: Identification of aldolase as a target antigen in Alzheimer's disease. J Immunol 2005, 175:3439–3445
50. Kishi H, Mukai T, Hirono A, Fujii H, Miwa S, Hori K: Human aldolase A deficiency associated with a hemolytic anemia: thermolabile aldolase due to a single base mutation. Proc Natl Acad Sci USA 1987, 84:8623–8627
51. Dandoy-Dron F, Benboudjema L, Guillo F, Jaegly A, Jasmin C, Dormont D, Tovey MG, Dron M: Enhanced levels of scrapie responsive gene mRNA in BSE-infected mouse brain. Brain Res Mol Brain Res 2000, 76:173–179
52. Dandoy-Dron F, Guillo F, Benboudjema L, Deslys JP, Lasmézas C, Dormont D, Tovey MG, Dron M: Gene expression in scrapie. Cloning of a new scrapie-responsive gene and the identification of increased levels of seven other mRNA transcripts. J Biol Chem 1998, 273:7691–7697
53. La Y, Wan C, Zhu H, Yang Y, Chen Y, Pan Y, Ji B, Feng G, He L: Hippocampus protein profiling reveals aberration of malate dehydrogenase in chlorpromazine/clozapine treated rats. Neurosci Lett 2006, 408:29–34
54. Gincel D, Zaid H, Shoshan-Barmatz V: Calcium binding and translocation by the voltage-dependent anion channel: a possible regulatory mechanism in mitochondrial function. Biochem J 2001, 358:147–155
55. Tsujimoto Y, Shimizu S: The voltage-dependent anion channel: an essential player in apoptosis. Biochimie 2002, 84:187–193
56. Jin JK, Kim NH, Min DS, Kim JI, Choi JK, Jeong BH, Choi SI, Choi EK, Carp RI, Kim YS: Increased expression of phospholipase D1 in the brains of scrapie-infected mice. J Neurochem 2005, 92:452–461
57. Carlier MF, Ressad F, Pantaloni D: Control of actin dynamics in cell motility. Role of ADF/cofilin. J Biol Chem 1999, 274:33827–33830
58. Jang DH, Han JH, Lee SH, Lee YS, Park H, Lee SH, Kim H, Kaang BK: Cofilin expression induces cofilin-actin rod formation and disrupts synaptic structure and function in Aplysia synapses. Proc Natl Acad Sci USA 2005, 102:16072–16077
59. Göthel SF, Marahiel MA: Peptidyl-prolyl cis-trans isomerases, a superfamily of ubiquitous folding catalysts. Cell Mol Life Sci 1999, 55:423–436
60. Immenschuh S, Baumgart-Vogt E: Peroxiredoxins, oxidative stress, and cell proliferation. Antioxid Redox Signal 2005, 7:768–777
61. Zabel C, Sagi D, Kaindl AM, Steireif N, Klare Y, Mao L, Peters H, Wacker MA, Kleene R, Klose J: Comparative proteomics in neurodegenerative and non-neurodegenerative diseases suggest nodal point proteins in regulatory networking. J Proteome Res 2006, 5:1948–1958

Highlighted paper selected by Editor-in-chief

Vitamin C Is Not Essential for Carnitine Biosynthesis *in Vivo*: Verification in Vitamin C-Depleted Senescence Marker Protein-30/Gluconolactonase Knockout Mice

Hajime Furusawa,[a,b,#] Yasunori Sato,[a,b,#] Yasukazu Tanaka,[c] Yoko Inai,[d] Akiko Amano,[b] Mizuki Iwama,[b] Yoshitaka Kondo,[b] Setsuko Handa,[b] Akira Murata,[e] Morimitsu Nishikimi,[d] Sataro Goto,[a,b] Naoki Maruyama,[b] Ryoya Takahashi,[a] and Akihito Ishigami*[,a,b]

[a] *Department of Biochemistry, Faculty of Pharmaceutical Sciences, Toho University; Chiba 274–8510, Japan:* [b] *Aging Regulation, Tokyo Metropolitan Institute of Gerontology;* [c] *Neuroscience and Brain Function, Tokyo Metropolitan Institute of Gerontology; Tokyo 173–0015, Japan:* [d] *Department of Biochemistry, Wakayama Medical University; Wakayama 641–0012, Japan: and* [e] *Department of Food and Nutrition, Saga Junior College; Saga 840–0806, Japan.*

Received May 24, 2008; accepted June 23, 2008; published online June 25, 2008

Carnitine is an essential cofactor in the transport of long-chain fatty acids into the mitochondrial matrix and plays an important role in energy production *via* β-oxidation. Vitamin C (VC) has long been considered a requirement for the activities of two enzymes in the carnitine biosynthetic pathway, *i.e.*, 6-*N*-trimethyllysine dioxygenase and γ-butyrobetaine dioxygenase. Our present study using senescence marker protein-30 (SMP30)/gluconolactonase (GNL) knockout (KO) mice, which cannot synthesize VC *in vivo*, led to the conclusion that this notion is not true. After weaning at 40 d of age, SMP30/GNL KO mice were fed a diet lacking VC and carnitine, then given water containing 1.5 g/l VC (VC(+) mice) or no VC (VC(−) mice) for 75 d. Subsequently, total VC and carnitine levels were measured in the cerebrum, cerebellum, liver, kidney, soleus muscle, extensor digitorum longus muscle, heart, plasma and serum. The total VC levels in all tissues and plasma from VC(−) SMP30/GNL KO mice were negligible, *i.e.*, <2% of the levels in SMP30/GNL KO VC(+) mice; however, the total carnitine levels of both groups were similar in all tissues and serum. In addition, carnitine was produced by incubated liver homogenates from the VC-depleted SMP30/GNL KO mice irrespective of the presence or absence of 1 mM VC. Collectively, these results indicate that VC is not essential for carnitine biosynthesis *in vivo*.

Key words ascorbic acid; gluconolactonase; vitamin C; senescence marker protein-30; butyrobetaine; dioxygenase

Carnitine (3-hydroxy-4-*N*-trimethylaminobutyric acid) is a metabolite essential for the transport of long-chain fatty acids from the cytosol into the mitochondrial matrix and is an important player in energy production *via* β-oxidation.[1—3] Therefore, carnitine depletion causes a failure of ATP production and an accumulation of triglycerides in tissues such as the liver, skeletal muscle and heart.[4—6] Animal tissues contain relatively large amounts of carnitine with the highest concentrations in heart and skeletal muscle.[7] Although animals obtain carnitine primarily from the diet, carnitine is also synthesized by most mammals but is not degraded in the body. Carnitine homeostasis in mammals is maintained by a modest rate of endogenous synthesis, absorption from dietary sources, efficient reabsorption in the kidney and mechanisms present in most tissues that establish and maintain substantial concentration gradients between intracellular and extracellular carnitine pools.[8]

Carnitine is synthesized ultimately from the amino acids lysine and methionine.[9—14] In some proteins (histones, myosin, calmodulin, and actin), lysine residues are trimethylated on the 4-amino group by specific methyltransferases that use *S*-adenosyl-L-methionine as the methyl donor[15] (Fig. 1). After lysosomal degradation of these proteins, free 6-*N*-trimethyllysine (TML)[6] becomes available for carnitine biosynthesis. Four enzymatic steps are required to synthesize carnitine, and the first and last steps are catalyzed by 6-*N*-trimethyllysine dioxygenase (TMLD, EC 1.14.11.8) and γ-butyrobetaine dioxygenase (γ-BBD, EC 1.14.11.1), respectively. TMLD hydroxylates TML on the 3-position to yield 3-hydroxy-TML (HTML),[16] and γ-BBD hydroxylates γ-butyrobetaine (γ-BB) on the 3-position to yield carnitine.[17] Both TMLD and γ-BBD are dioxygenases; hydroxylation of their substrates is coupled to the conversion of 2-oxoglutarate and molecular oxygen to succinate and carbon dioxide. In addition, the TMLD protein shows high homology to the γ-BBD protein, although they appear to belong to separate subfamilies of the 2-oxoglutarate-dependent dioxygenases.[3] TMLD is associated predominantly with mitochondria,[18,19] whereas γ-BBD is localized in the cytosol.[20,21] Although γ-BBD activity has been detected in kidneys from humans, cats, cows, hamsters, rabbits and Rhesus monkeys at equal or higher levels than that in the liver, the activity was not detectable or detected at very low levels in kidneys from Cebus monkeys, sheep, dogs, guinea pigs, mice and rats, in which γ-BBD activity predominates in the liver.[22—24]

In 1962, Lindstedts[25] first showed that γ-BBD is stimulated considerably by 2-oxoglutarate and that the enzyme requires molecular oxygen, reduced iron (Fe^{2+}) and vitamin C (VC, L-ascorbic acid) for enzyme activity. Therefore, many studies reported the enhancement of γ-BBD and TMLD activity upon the addition of VC in a dose-dependent manner using tissue extracts or partially purified enzymes.[18—22,26—28] In the absence of VC, however, γ-BBD activity was detected by adding glutathione peroxidase and glutathione (GSH) to the reaction mixture,[29] although this test was not performed for TMLD.

To ascertain the necessity of VC for γ-BBD and TMLD activity in carnitine biosynthesis, researchers used guinea pigs that, like humans, cannot synthesize VC *in vivo*. Many reports indicated that carnitine levels, especially in tissues

* To whom correspondence should be addressed. e-mail: ishigami@phar.toho-u.ac.jp

# These authors contributed equally to this work.

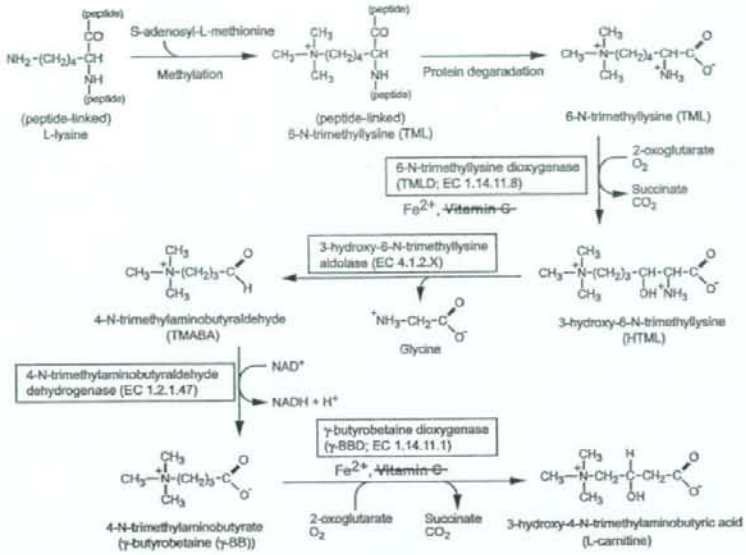

Fig. 1. The Pathway of Carnitine Biosynthesis with Proposed Involvement of VC

L-Lysine residues in proteins are trimethylated by specific methyltransferases that use *S*-adenosyl-L-methionine as the methyl donor to TML. After its release by protein degradation, TML is hydroxylated by TMLD to HTML. HTML is cleaved by 3-hydroxy-6-*N*-trimethyllysine aldolase to 4-*N*-trimethylaminobutyraldehyde (TMABA) and glycine. TMABA is oxidized to γ-BB by 4-*N*-trimethylaminobutyraldehyde dehydrogenase. In the last step, γ-BB is hydroxylated to L-carnitine by γ-BBD. In the present study, we found VC is not an essential cofactor for the activation of γ-BBD and TMLD in the carnitine biosynthesis pathway.

where carnitine is the most abundant such as the heart and skeletal muscle, decreased significantly when the animals became depleted in VC. Since then, VC has been deemed essential for γ-BBD and TMLD activity.[30—32] However, in 1990 Alkonyi *et al.*[33] reported that an increase in urinary excretion contributed greatly to a carnitine deficiency in guinea pigs during states of VC deficiency and starvation. Rebouche[34] also reported that the carnitine depletion related to a VC deficiency results from a decrease in carnitine reabsorption. Thus, since the VC status of such animals influences their urinary excretion of carnitine, guinea pigs are not appropriate subjects for use in studies of carnitine biosynthesis to determine the involvement of VC.

Recently we have established senescence marker protein 30 (SMP30)/gluconolactonase (GNL) knockout (KO) mice, which are incapable of synthesizing VC *in vivo*, because SMP30/GNL is involved in the VC biosynthetic pathway.[35] SMP30/GNL KO mice are actually subject to scurvy when fed a VC-deficient diet.[35] Therefore, in this study, we used VC-depleted SMP30/GNL KO mice to determine the necessity of VC for carnitine biosynthesis *in vivo* and *in vitro*.

MATERIALS AND METHODS

Animals SMP30/GNL KO mice were previously generated by the gene targeting technique.[36] Heterozygous female mice (*SMP30/GNL*$^{+/-}$) were mated with male KO mice (*SMP30/GNL*$^{Y/-}$) to produce male KO (*SMP30/GNL*$^{Y/-}$) and male wild-type (WT) (*SMP30/GNL*$^{Y/+}$) littermates. Heterozygous male mice do not exist, because the SMP30/GNL gene is located on the X chromosome. Genotypes of SMP30/GNL mutant mice were determined as described previously.[36] SMP30/GNL KO and WT mice were weaned at 40 d of age, at which time they were divided into the following four groups: VC [VC(+)], VC-free [VC(−)], WT and SMP30/GNL KO mice. The VC(+) group had free access to water containing VC (1.5 g/l) and 10 μM EDTA, whereas the VC(−) group had free access to water without VC. Water bottles were changed every 3 or 4 d until the experiment ended. After weaning, all mice were fed a VC- and carnitine-deficient diet (CLEA-purified diet; CLEA Japan, Tokyo, Japan), the composition of which is listed in Table 1. Throughout the experiments, animals were maintained on a 12-h light/dark cycle in a controlled environment. All experimental procedures using laboratory animals were approved by the Animal Care and Use Committee of the Tokyo Metropolitan Institute of Gerontology.

Measurement of VC VC in tissues and plasma was measured by a high-performance liquid chromatography (HPLC)-electrochemical detection (ECD) method. Tissues were homogenized in 14 volumes of 5.4% metaphosphate and centrifuged at 21000 ***g*** for 10 min at 4 °C. Plasma was mixed with nine volumes of 20% metaphosphate and centrifuged at 21000 ***g*** for 10 min at 4 °C. The supernatants obtained were kept at −80 °C until use. Samples were analyzed by HPLC using an Atlantis dC18 5 μm column (4.6×150 mm, Nihon Waters, Tokyo, Japan). The mobile phase was 50 mM phosphate buffer (pH 2.8), 0.2 g/l EDTA, 2% methanol at flow rate of 1.3 ml/min, and electrical signals were recorded by using an electrochemical detector with a glassy carbon electrode at +0.6 V.[37,38]

Measurement of Total Carnitine Tissues were homogenized in 100 volumes of 0.14 M NaCl and centrifuged at 9600 ***g*** for 10 min at 4 °C. Serum was centrifuged at 9600 ***g*** for 10 min at 4 °C. The supernatants obtained after centrifugation were kept at −80 °C until use. The total carnitine

Table 1. Diet Composition of CLEA-Purified Diet

Nutritional component (in 100 g)	
Moisture (g)	8.0
Crude protein (g)	20.4
Crude fat (g)	6.0
Crude fiber	3.0
Crude ash (g)	6.2
Nitrogen-free extract (NFE) (g)	56.4
Calorie (kcal)	361.2
Minerals (in 100 g)	
Ca (g)	0.89
P (g)	0.66
Mg (g)	0.08
Na (g)	0.23
K (g)	0.50
Fe (mg)	31.70
Cu (mg)	0.32
Zn (mg)	3.46
Co (mg)	0.10
Mn (mg)	3.51
Vitamins (in 100 g)	
Vitamin A (mg)	1.65
Vitamin D_3 (μg)	25
Vitamin E (mg)	20
Vitamin K_3 (mg)	0.3
Vitamin B_1 (mg)	1.5
Vitamin B_2 (mg)	1.6
Vitamin C (mg)[a)]	ND
Vitamin B_6 (mg)	1.0
Vitamin B_{12} (μg)	0.5
Pantothenic acid (mg)	4.0
Niacin (nicotinic acid) (mg)	10.2
Folic acid (mg)	0.2
Choline (mg)	300
Biotin (μg)	500
Inositol (mg)	15
Other component (in 100 g)	
Total carnitine (mg)[a)]	ND

ND, not detectable. Data from CLEA Japan, Tokyo, Japan. *a*) VC and total carnitine were measured as described in Materials and Methods.

(acyl carnitine plus free carnitine) levels in tissues and serum were measured by using an enzyme cycling method with carnitine dehydrogenase.[39] For this, Total Carnitine Kainos (Kainos Laboratories, Tokyo, Japan) was used.

Measurement of Carnitine Urinary Excretion For measurement of carnitine excreted into urine, a mouse was housed in a metabolic cage, and urine was collected for 24 h in a bottle containing mineral oil to prevent evaporation. This urine was centrifuged at 21000 ***g*** for 10 min at 4 °C and kept at −80 °C until use. The total carnitine (acyl carnitine plus free carnitine) levels in urine were measured using Total Carnitine Kainos. Creatinin levels in urine were measured using a Creatinin Test Wako kit (Wako Pure Chemical, Osaka, Japan) according to the manufacturer's instruction, and carnitine levels were normalized by creatinin value.

In Vitro* Carnitine Biosynthesis Assay** After SMP30/GNL KO mice were weaned at 40 d of age, they were fed a carnitine- and VC-deficient diet and water without VC for 75 d. These mice were then sacrificed; their livers and kidneys were collected and homogenized in 10 mM Tris–HCl (pH 7.6) containing 1 mM phenylmethylsulfonyl fluoride. For the carnitine biosynthesis assay, the homogenates were incubated in the presence or absence of 1 mM VC at 37 °C for 15, 30, 45, 60, and 90 min. The reaction was stopped by immediate transfer of sample tubes into an ice water bath, and the samples were quickly frozen on dry ice. For the measurement of VC, aliquots of the reaction mixtures were mixed with an equal volume of 10% metaphosphate, and the VC levels were measured by the HPLC-ECD methods described above. For the measurement of carnitine, aliquots of the reaction mixtures were centrifuged at 21000 ***g for 10 min at 4 °C, and the total carnitine levels in the supernatants were measured by using Total Carnitine Kainos. The protein concentration was determined by the BCA protein assay (Pierce Biotechnology, Inc., Rockford, IL, U.S.A.) using bovine serum albumin as a standard.

Measurement of Glutathione (GSH) The GSH levels in tissues and plasma were measured by HPLC.[40] Tissues were homogenized in nine volumes of 1 M perchloric acid (PCA) and centrifuged at 21000 ***g*** for 30 min at 4 °C. Plasma samples were mixed with one volume of 1 M PCA and centrifuged at 21000 ***g*** for 10 min at 4 °C. The supernatants obtained were kept at −80 °C until use. The GSH in samples was analyzed by HPLC, using a Sun Fire column (4.6×150 mm, Nihon Waters, Tokyo, Japan). The mobile phase was 0.1 M sodium perchlorate monohydrate, 5% acetonitrile, 0.05% trifluoroacetate at a flow rate of 0.5 ml/min, and the absorbance at 220 nm was recorded.

Statistical Analysis Results are expressed as means±S.E.M. The probability of statistical differences between experimental groups was determined by Student's *t*-test or ANOVA as appropriate. For one- and two-way ANOVAs, we used KaleidaGraph software (Synergy Software, Reading, PA, U.S.A.). Statistical differences were considered significant at $p<0.05$.

RESULTS

Body Weight Change To investigate, the effect of VC on growth, we compared one group of SMP30/GNL KO mice fed drinking water containing 1.5 g/l VC [VC(+)] with an identical group given water without VC [VC(−)]. The VC(−) mice initially gained weight to the same degree as the VC(+) mice. However, the mean body weight of VC(−) SMP30/GNL KO mice gradually decreased starting at 40 d after weaning (Fig. 2). The mean body weights of the VC(+) and VC(−) KO mice at 70 d after weaning were 35.2±1.7 g and 23.9±1.9 g, respectively, the weight of VC(−) KO mice being less by 32% than that of VC(+) KO mice. Mean water consumption during the experiment was not significantly different between the two groups, *i.e.*, 3.6±0.3 ml/d/mouse for VC(+) KO mice and 3.2±0.5 ml/d/mouse for VC(−) KO mice. Throughout the experiment, the increase with time in body weight of VC(+) SMP30/GNL KO mice was similar to those of VC(+) and VC(−) WT mice that were tested for comparison.

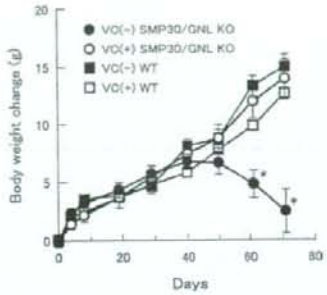

Fig. 2. Body Weight Changes of VC(+) and VC(−) Groups Composed of WT and SMP30/GNL KO Mice

After the mice were weaned at 40 d of age (indicated at day 0), their body weights were measured for 75 d, and the mean body weight changes (difference from the mean body weight at day 0) were plotted. The final body weights of VC(+) SMP30/GNL KO, VC(−) SMP30/GNL KO, VC(+) WT and VC(−) WT mice at day 70 were 35.2±1.7 g, 23.9±1.9 g, 33.9±0.5 g and 39.1±0.5 g, respectively. Values are expressed as means±S.E.M. of five animals. * $p<0.01$ as compared to other three groups.

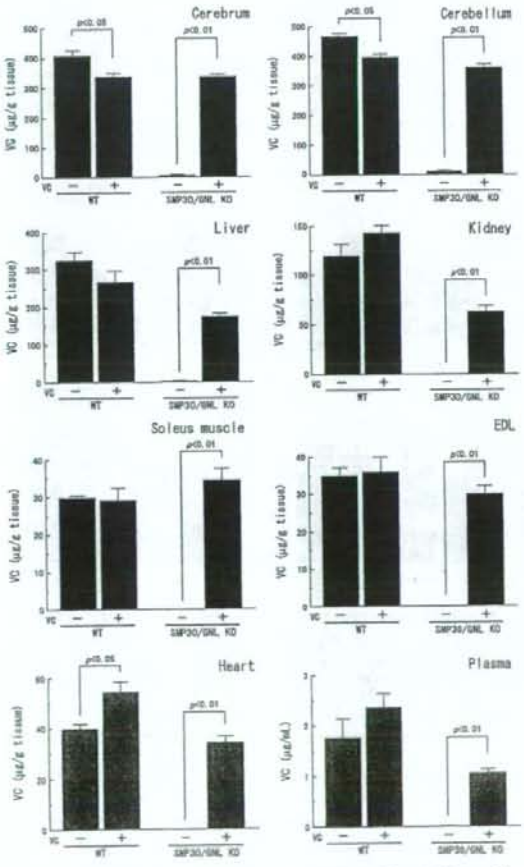

Fig. 3. VC Levels in the Cerebrum, Cerebellum, Liver, Kidney, Soleus Muscle, Extensor Digitorum Longus Muscle (EDL), Heart and Plasma from VC(+) and VC(−) Groups from WT and SMP30/GNL KO Mice

Mice were supplied with or deprived of VC in drinking water for 75 d, starting when they were weaned at 40 d of age. Values of VC are expressed as means±S.E.M. of five animals.

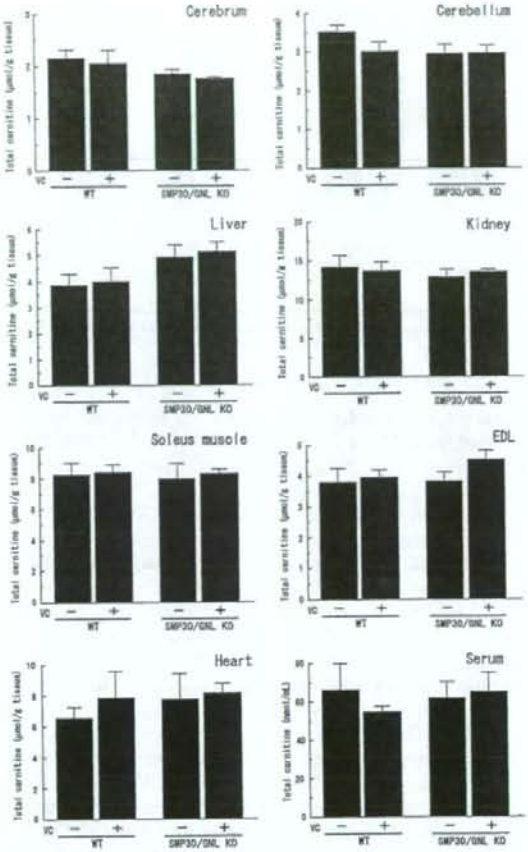

Fig. 4. Total Carnitine Levels in the Cerebrum, Cerebellum, Liver, Kidney, Soleus Muscle, Extensor Digitorum Longus Muscle (EDL), Heart and Serum from VC(+) and VC(−) Groups of WT and SMP30/GNL KO Mice

Mice were supplied with or deprived of VC in drinking water for 75 d, starting when they were weaned at 40 d of age. Values of total carnitine are expressed as means±S.E.M. of five animals.

Total VC and Carnitine Levels in Tissues after VC Depletion To examine the VC status in the VC(−) SMP30/GNL KO mice, we determined the quantity of VC in the cerebrum, cerebellum, liver, kidney, soleus muscle, extensor digitorum longus (EDL) muscle, heart and plasma at 75 d after weaning. The VC levels in all these tissues and plasma from VC(−) SMP30/GNL KO mice were <2% of the values obtained for the VC(+) SMP30/GNL KO mice (Fig. 3). Most of the latter values were similar to those of VC(+) and VC(−) WT mice. However, in the liver, kidney and plasma, VC levels of VC(+) mice were approximately half of those in the VC(+) and VC(−) WT mice.

Total carnitine (acyl carnitine plus free carnitine) levels in the cerebrum, cerebellum, liver, kidney, soleus muscle, EDL muscle, heart and serum at 75 d after weaning are shown in Fig. 4. No significant difference was noted in any of these tissues from VC(−) and VC(+) SMP30 KO mice. Moreover, the total carnitine levels of these two groups were not significantly different from those observed for VC(−) and VC(+)

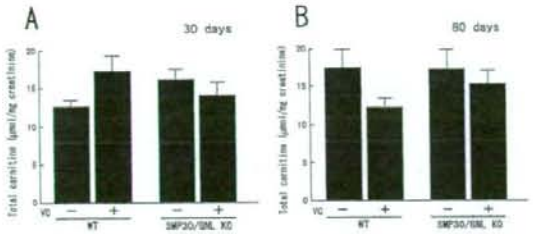

Fig. 5. Excretion of Total Carnitine in the Urine at (A) 30 d and (B) 80 d after Weaning of VC(+) and VC(−) Groups of WT and SMP30/GNL KO Mice

Each mouse was housed in a metabolic cage, and urine was collected for 24 h. Values of total carnitine were normalized by crestinin values and expressed as means±S.E.M. of five animals.

WT mice.

Urinary Carnitine Excretion upon VC Depletion Rebouche[34] reported that carnitine depletion in VC-deficient guinea pigs results from the decreased efficiency of carnitine reabsorption in kidney. To examine whether a VC deficiency influences urinary excretion of carnitine in SMP30/GNL KO mice, we measured the urinary carnitine from VC(−) SMP30/GNL KO mice and their VC(+) counterparts. At 30 and 80 d after weaning, both groups were evaluated for total carnitine levels in 24-h urine samples (Fig. 5), but no significant difference was found. The urinary carnitine contents of VC(−) and VC(+) WT mice were also similar.

***In Vitro* Carnitine Biosynthesis Assay** For this assay, we used liver and kidney homogenates originating from VC(−) SMP30/GNL KO mice at 75 d after weaning. Liver homogenates contained endogenous enzymes for carnitine biosynthesis and had no detectable level of VC. When the liver homogenates were incubated at 37 °C, the concentration of carnitine increased time-dependently for 60 min and then gradually decreased (Fig. 6A). Addition of 1 mM VC did not affect the course of that carnitine formation. On the other hand, the carnitine levels in kidney homogenates were not changed until 90 min of culture even when VC was added (Fig. 6B). To validate this assay system, we heated liver homogenates at 95 °C for 5 min and then performed the carnitine biosynthesis assay. However, the carnitine levels did not change at all during incubation for 120 min (Fig. 6C).

Tissue GSH Levels after VC Depletion GSH levels were then compared in the liver, soleus muscle, heart and serum from all four groups of test mice at 75 d after weaning. In livers from VC(−) SMP30/GNL KO mice, amounts of GSH were increased by 44.5%, 32.8% and 30.8%, respectively, above levels in livers from VC(+) SMP30/GNL KO, VC(+) WT and VC(−) WT mice, but the differences among the four groups were not statistically significant (Fig. 7). On the other hand, GSH levels in the soleus muscles and plasma from VC(−) SMP30/GNL KO mice were 30.8% and 45.5%, respectively, lower than in VC(+) SMP30/GNL KO mice, although the GSH content in heart tissues from VC(−) SMP30/GNL KO mice were not changed when compared to the other three groups.

DISCUSSION

Despite the traditional belief that VC is an essential cofactor for the activation of γ-BBD and TMLD in the carnitine biosynthesis pathway *in vivo*, results from the present study using VC-depleted SMP30/GNL KO mice challenge this assumption. Our conclusion to the contrary stems from experiments presented here in which these VC(−) SMP30/GNL KO mice successfully produced carnitine despite the animals' VC insufficiency.

SMP30 is an age-associated protein that decreases with aging in the liver, kidney and lungs in an androgen-independent manner.[41–43] SMP30 was first discovered in 1992 by

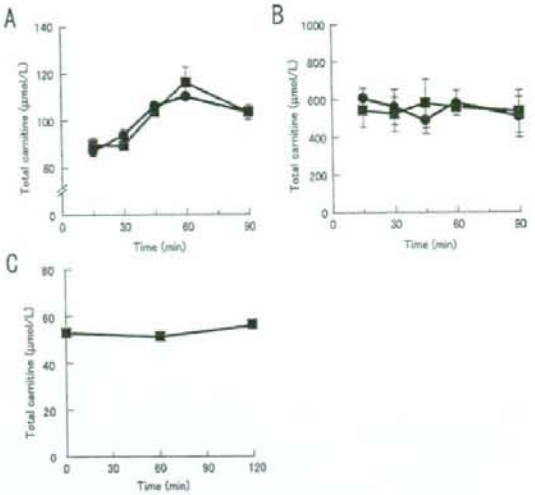

Fig. 6. *In Vitro* Carnitine Biosynthesis Assay

VC-depleted liver and kidney homogenates were prepared as described in Materials and Methods. For the carnitine biosynthesis assay, homogenates were incubated with 1 mM VC (closed circle) or without VC (closed square) at 37 °C for the indicated times. (A) Total carnitine concentrations in liver homogenates during incubation. (B) Total carnitine concentrations in kidney homogenates during incubation. (C) Total carnitine concentrations in VC-depleted liver homogenates heated at 95 °C for 5 min then incubated at 37 °C for 60 and 120 min. Values are expressed as means±S.E.M. of four samples.

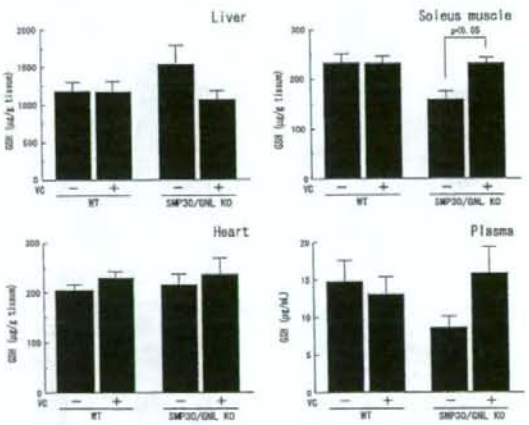

Fig. 7. GSH Levels in the Liver, Soleus Muscle, Heart and Plasma from VC(+) and VC(−) Groups from WT and SMP30/GNL KO Mice

Mice were supplied with or deprived of VC in drinking water for 75 d, starting when they were weaned at 40 d of age. Values of GSH are expressed as means±S.E.M. of five animals.

using a proteomic analysis that compared soluble proteins from the livers of young and old rats.[41] Although the decreased expression of SMP30 during aging was immediately apparent, the physiological functions of SMP30 remained obscure for more than ten years.[44] To resolve this issue, we developed SMP30 KO mice by gene targeting.[36] During subsequent experiments performed *in vivo* and *in vitro*, SMP30 KO mice proved far more susceptible to TNF-α- and Fas-mediated apoptosis than their WT counterparts[36] and showed abnormal accumulations of lipids including triglycerides, cholesterol and phospholipids in the liver.[45,46] Recently we found that SMP30 is a GNL involved in the VC biosynthetic pathway. Further study showed that SMP30/GNL KO mice could not synthesize VC *in vivo* and that they developed symptoms of scurvy when fed a VC-deficient diet.[35]

The SMP30/GNL KO mice used here were fed a VC- and carnitine-deficient diet (Table 1) and water containing no VC for 75 d after weaning, which began when the animals were 40-d-old. Initially, these VC(−) SMP30/GNL KO mice grew as well as matching VC(+) mice as evident from their increased body weight for the first 40 d followed by a gradual decrease (Fig. 2). After another 30 d, the VC(−) KO mice weighed 32% less than the VC(+) controls given supplementary VC. Additionally, multiple tissues and plasma of the SMP30/GNL KO mice had less than 2% the VC content of VC(+) SMP30/GNL KO, VC(+) WT and VC(−) WT mice (Fig. 3). However, total carnitine levels in various tissues and serum unexpectedly showed no difference among these four groups (Fig. 4). The abundance of carnitine in the heart and skeletal muscle has been attributed to these tissues' production of energy *via* β-oxidation from long-chain fatty acids for muscle expansion.[7]

In mammals, carnitine homeostasis is maintained by adsorption from dietary sources, endogenous synthesis and efficient tubular reabsorption by the kidney. *In vivo*, VC depletion in tissues and plasma may be a manifestation of the inhibitory effects of carnitine excretion from tissues and an increase in the efficiency of tubular reabsorption from the kidney. To examine the effects of VC depletion and carnitine deficiency on the urinary excretion of carnitine, we measured total carnitine levels in urine collected for 24 h periods at 30 and 80 d after feeding of a VC- and carnitine-deficient diet. However, the total carnitine levels in urine were quite similar in all four groups of test mice at those time intervals (Fig. 5). These results denote that the VC deficiency in tissues and plasma had no influence on the urinary carnitine excretion of SMP30/GNL KO mice.

However, many reports indicate that tissue carnitine levels are significantly decreased in VC-depleted guinea pigs *in vivo*.[30—32] Alkonyi *et al.*[33] reported that an increase of urinary excretion greatly contributed to the loss of carnitine in guinea pigs during states of VC deficiency and starvation. Rebouche[34] also stated that carnitine depletion in VC-deficient guinea pigs resulted from a decreased efficiency of carnitine reabsorption in their kidneys. These reports strongly assert that subnormal levels of VC in various tissues of VC-depleted guinea pigs were caused by a rise in urinary carnitine excretion. If so, guinea pigs cannot be used to determine the involvement of VC in carnitine biosynthesis. In the present study the amount of carnitine excreted in the urine of SMP30/GNL KO mice was no different in samples from VC-depleted *versus* VC-supplemented animals (Fig. 5). Although the difference between guinea pigs and SMP30/GNL KO mice is still unclear, SMP30/GNL KO mice are a far more suitable animal model for determining the necessity of VC in carnitine biosynthesis.

We further examined carnitine biosynthesis by using VC-depleted liver and kidney tissues from SMP30/GNL KO mice. Humans, cats, cows, hamsters and rabbits can synthesize carnitine in the liver and kidney because they have γ-BBD activity in those tissues; however, mice, rats, sheep, dogs and guinea pigs synthesize carnitine only in the liver, because their kidneys lack γ-BBD activity entirely or contain only very low levels.[22—24] In the present study of liver homogenates from VC-depleted SMP30/GNL KO mice with and without 1 mM VC, there was no difference in carnitine production (Fig. 6A). In addition, no carnitine production was detectable in the kidney samples according to the same assay system (Fig. 6B). These results strongly suggest that VC is not essential for carnitine biosynthesis *in vitro*. Vlies *et al.*[24] reported that both TMLD and γ-BBD activities were reduced when VC was removed from their complete assay mixture *in vitro*. However, Punekar *et al.*[29] observed a small amount of carnitine synthesis, but not VC, in the presence of GSH, in their assay mixture. Further, a combination of GSH and glutathione peroxidase yielded a large amount of carnitine synthesis, suggesting that GSH may effectively replace VC in the carnitine biosynthetic pathway. In the present study, in the livers from our VC(−) SMP30/GNL KO mice, GSH levels were higher by 31 to 45% than in those from the other three groups tested, although the difference was not statistically significant (Fig. 7). Conversely, GSH levels in soleus muscles and plasma of VC(−) SMP30/GNL KO mice were lower than that from the other three groups. The low GSH levels in soleus muscles and plasma of VC(−) SMP30/GNL KO mice supposed that GSH is utilized to carnitine synthesis in the liver and consequently decreased distribution and storage levels in other tissues. These results reinforce the likelihood that GSH may replace VC in the carnitine biosynthetic pathway *in vivo* when VC is depleted in liver.

In conclusion, our results indicate that VC is not essential for carnitine biosynthesis *in vivo*, as verified by the clearcut presence of carnitine in VC-depleted SMP30/GNL KO mice. Additionally, GSH may compensate for VC in the event of the latter's depletion. Finally, our model of SMP30/GNL KO mice provides an optimal opportunity for investigating the necessity of VC in carnitine biosynthesis.

Acknowledgements This study is supported by a Grant-in-Aid for Scientific Research from the Ministry of Education, Culture, Sports, Science and Technology of Japan (to A.I., S.H., and N.M.), a grant from Health Science Research Grants for Comprehensive Research on Aging and Health supported by the Ministry of Health, Labor, and Welfare, Japan (to N.M.), and a Grant-in-Aid for Smoking Research Foundation, Japan (to A.I.) and the Suzuken Memorial Foundation, Japan (to A.I.). We thank Ms. P. Minick for the excellent English editorial assistance. Vitamin C powder was kindly provided by DSM Nutrition Japan.

REFERENCES

1) Ramsay R. R., Gandour R. D., van der Leij F. R., *Biochim. Biophys. Acta*, **1546**, 21—43 (2001).
2) Fritz I. B., Yue K. T., *J. Lipid Res.*, **4**, 279—288 (1963).
3) Vaz F. M., Wanders R. J., *Biochem J.*, **361**, 417—429 (2002).
4) Breningstall G. N., *Pediatr. Neurol.*, **6**, 75—81 (1990).
5) Suenaga M., Kuwajima M., Himeda T., Morokami K., Matsuura T., Ozaki K., Arakaki N., Shibata, H., Higuti, T., *Biol. Pharm. Bull.*, **27**, 496—503 (2004).
6) Kuwajima M., Lu K., Sei M., Ono A., Hayashi M., Ishiguro K., Ozaki K., Hotta K., Okita K., Murakami T., Miyagawa J., Narama I., Nikaido H., Hayakawa J., Nakajima H., Namba M., Hanafusa T., Matsuzawa Y., Shima K., *J. Mol. Cell. Cardiol.*, **30**, 773—781 (1998).
7) Bremer J., *Physiol. Rev.*, **63**, 1420—1480 (1983).
8) Rebouche C. J., Seim H., *Annu. Rev. Nutr.*, **18**, 39—61 (1998).
9) Horne D. W., Tanphaichitr V., Broquist H. P., *J. Biol. Chem.*, **246**, 4373—4375 (1971).
10) Tanphaichitr V., Horne D. W., Broquist H. P., *J. Biol. Chem.*, **246**, 6364—6366 (1971).
11) Cox R. A., Hoppel C. L., *Biochem. J.*, **136**, 1083—1090 (1973).
12) Cox R. A., Hoppel C. L., *Biochem. J.*, **136**, 1075—1082 (1973).
13) Horne D. W., Broquist H. P., *J. Biol. Chem.*, **248**, 2170—2175 (1973).
14) Tanphaichitr V., Broquist H. P., *J. Biol. Chem.*, **248**, 2176—2181 (1973).
15) Paik W. K., Kim S., *Science*, **174**, 114—119 (1971).
16) Hoppel C. L., Cox R. A., Novak R. F., *Biochem. J.*, **188**, 509—519 (1980).
17) Lindstedt G., Lindstedt S., *J. Biol. Chem.*, **240**, 316—321 (1965).
18) Hulse J. D., Ellis S. R., Henderson L. M., *J. Biol. Chem.*, **253**, 1654—1659 (1978).
19) Sachan D. S., Broquist H. P., *Biochem. Biophys. Res. Commun.*, **96**, 870—875 (1980).
20) Lindstedt G., *Biochemistry*, **6**, 1271—1282 (1967).
21) Lindstedt G., Lindstedt S., *J. Biol. Chem.*, **245**, 4178—4186 (1970).
22) Englard S., Carnicero H. H., *Arch. Biochem. Biophys.*, **190**, 361—364 (1978).
23) Englard S., *FEBS Lett.*, **102**, 297—300 (1979).
24) van Vlies N., Wanders R. J., Vaz F. M., *Anal. Biochem.*, **354**, 132—139 (2006).
25) Lindstedt G., Lindstedt S., *Biochem. Biophys. Res. Commun.*, **7**, 394—397 (1962).
26) Lindstedt G., Lindstedt S., Tofft M., *Biochemistry*, **9**, 4336—4342 (1970).
27) Englard S., Horwitz L. J., Mills J. T., *J. Lipid Res.*, **19**, 1057—1063 (1978).
28) Kondo A., Blanchard J. S., Englard S., *Arch. Biochem. Biophys.*, **212**, 338—346 (1981).
29) Punekar N. S., Wehbie R. S., Lardy H. A., *J. Biol. Chem.*, **262**, 6720—6724 (1987).
30) Hughes R. E., Hurley R. J., Jones E., *Br. J. Nutr.*, **43**, 385—387 (1980).
31) Nelson P. J., Pruitt R. E., Henderson L. L., Jenness R., Henderson L. M., *Biochim. Biophys. Acta*, **672**, 123—127 (1981).
32) Dunn W. A., Rettura G., Seifter E., Englard S., *J. Biol. Chem.*, **259**, 10764—10770 (1984).
33) Alkonyi I., Cseko J., Sandor A., *J. Clin. Chem. Clin. Biochem.*, **28**, 319—321 (1990).
34) Rebouche C. J., *Metabolism*, **44**, 1639—1643 (1995).
35) Kondo Y., Inai Y., Sato Y., Handa S., Kubo S., Shimokado K., Goto S., Nishikimi M., Maruyama N., Ishigami A., *Proc. Natl. Acad. Sci. U.S.A.*, **103**, 5723—5728 (2006).
36) Ishigami A., Fujita T., Handa S., Shirasawa T., Koseki H., Kitamura T., Enomoto N., Sato N., Shimosawa T., Maruyama N., *Am. J. Pathol.*, **161**, 1273—1281 (2002).
37) Margolis S. A., Davis T. P., *Clin. Chem.*, **34**, 2217—2223 (1988).
38) Margolis S. A., Paule R. C., Ziegler R. G., *Clin. Chem.*, **36**, 1750—1755 (1990).
39) Takahashi M., Ueda S., Misaki H., Sugiyama N., Matsumoto K., Matsuo N., Murao S., *Clin. Chem.*, **40**, 817—821 (1994).
40) Reed D. J., Babson J. R., Beatty P. W., Brodie A. E., Ellis W. W., Potter D. W., *Anal. Biochem.*, **106**, 55—62 (1980).
41) Fujita T., Uchida K., Maruyama N., *Biochim. Biophys. Acta*, **1116**, 122—128 (1992).
42) Ishigami A., Maruyama N., *Geriatr. Gerontol. Int.*, **7**, 316—325 (2007).
43) Maruyama N., Ishigami A., Kuramoto M., Handa S., Kubo S., Imasawa T., Seyama K., Shimosawa T., Kasahara Y., *Ann. N.Y. Acad. Sci.*, **1019**, 383—387 (2004).
44) Kondo Y., Ishigami A., Kubo S., Handa S., Gomi K., Hirokawa K., Kajiyama N., Chiba T., Shimokado K., Maruyama N., *FEBS Lett.*, **570**, 57—62 (2004).
45) Ishigami A., Kondo Y., Nanba R., Ohsawa T., Handa S., Kubo S., Akita M., Maruyama N., *Biochem. Biophys. Res. Commun.*, **315**, 575—580 (2004).
46) Son T. G., Zou Y., Jung K. J., Yu B. P., Ishigami A., Maruyama N., Lee J., *Mech. Ageing Dev.*, **127**, 451—457 (2006).

Biochemical and Biophysical Research Communications 375 (2008) 346–350

Contents lists available at ScienceDirect

Biochemical and Biophysical Research Communications

journal homepage: www.elsevier.com/locate/ybbrc

Hydrogen-rich pure water prevents superoxide formation in brain slices of vitamin C-depleted SMP30/GNL knockout mice

Yasunori Sato [a,b,1], Shizuo Kajiyama [c,1], Akiko Amano [b], Yoshitaka Kondo [b], Toru Sasaki [d], Setsuko Handa [b], Ryoya Takahashi [a], Michiaki Fukui [e], Goji Hasegawa [e], Naoto Nakamura [e], Hikohito Fujinawa [f], Toyotaka Mori [f], Mitsuhiro Ohta [g], Hiroshi Obayashi [h], Naoki Maruyama [b], Akihito Ishigami [a,b,*]

[a] Department of Biochemistry, Faculty of Pharmaceutical Sciences, Toho University, Chiba 274-8510, Japan
[b] Aging Regulation, Tokyo Metropolitan Institute of Gerontology, Tokyo 173-0015, Japan
[c] Kajiyama Clinic, Kyoto 615-0035, Japan
[d] Research Team for Molecular Biomarker, Tokyo Metropolitan Institute of Gerontology, Tokyo 173-0015, Japan
[e] Department of Endocrinology and Metabolism, Kyoto Prefectural University of Medicine, Graduate School of Medical Science, Kyoto 602-8566, Japan
[f] Trom Pharmaceutical Co., LTD., Tokyo 141-0032, Japan
[g] Department of Medical Biochemistry, Kobe Pharmaceutical University, Kobe 658-8566, Japan
[h] Institute of Bio-Response Informatics, Kyoto 612-8016, Japan

ARTICLE INFO

Article history:
Received 31 July 2008
Available online 14 August 2008

Keywords:
Ascorbic acid
Chemiluminescence
Gluconolactonase
Hydrogen-rich pure water
Oxidative stress
ROS
Senescence marker protein-30
Superoxide
Vitamin C

ABSTRACT

Hydrogen is an established anti-oxidant that prevents acute oxidative stress. To clarify the mechanism of hydrogen's effect in the brain, we administered hydrogen-rich pure water (H_2) to senescence marker protein-30 (SMP30)/gluconolactonase (GNL) knockout (KO) mice, which cannot synthesize vitamin C (VC), also a well-known anti-oxidant. These KO mice were divided into three groups; recipients of H_2, VC, or pure water (H_2O), administered for 33 days. VC levels in H_2 and H_2O groups were <6% of those in the VC group. Subsequently, superoxide formation during hypoxia-reoxygenation treatment of brain slices from these groups was estimated by a real-time biography imaging system, which models living brain tissues, with Lucigenin used as chemiluminescence probe for superoxide. A significant 27.2% less superoxide formed in the H_2 group subjected to ischemia–reperfusion than in the H_2O group. Thus hydrogen-rich pure water acts as an anti-oxidant in the brain slices and prevents superoxide formation.

The production of reactive oxygen species (ROS) and reduction of anti-oxidant defense systems are major causes of oxidative stress [1]. Oxidative stress has been associated with the physiologic degeneration that accompanies Alzheimer's and Parkinson's diseases [2], cardiovascular disease [3], diabetes [4], and aging [5,6]. Exposure to ROS from a variety of sources has led organisms to develop multiple defense mechanisms such as enzymatic and non-enzymatic anti-oxidants [7]. Superoxide dismutase, glutathione peroxidase, and catalase are major enzymatic anti-oxidants, whereas vitamin C (VC, L-ascorbic acid), vitamin E (α-tocopherol), and glutathione are the main non-enzymatic anti-oxidants. However, VC is a particularly important anti-oxidant in the brain, which is richer in VC content than other tissues.

Although most organisms have developed anti-oxidant defense systems, not all excess ROS are detoxified. In 1997, Shirahata et al. [8] reported that electrolyzed-reduced water, which dissolved large amounts of hydrogen, had the ability to protect DNA from oxidative damage. Recently, Ohsawa et al. [9] found that hydrogen acts as a therapeutic anti-oxidant by selectively reducing hydroxyl radicals (·OH). We also described an improvement of lipid and glucose metabolism after supplementation with hydrogen-rich pure water in patients with type 2 diabetes or impaired glucose tolerance [10]. These findings strongly indicate that hydrogen has anti-oxidant ability *in vivo* and provides protection from the oxidative stress associated with numerous diseases. However, the specific mechanism of hydrogen's ability to scavenge ROS *in vivo* is still unclear.

Abbreviations: EDTA, ethylenediaminetetraacetic acid; GNL, gluconolactonase; HPLC, high-performance liquid chromatography; KO, knockout; ROS, reactive oxygen species; SMP30, senescence marker protein-30; SOD, superoxide dismutase; VC, vitamin C.

* Corresponding author. Address: Department of Biochemistry, Faculty of Pharmaceutical Sciences, Toho University, Chiba 274-8510, Japan. Fax: +81 47 472 1536.
E-mail address: ishigami@phar.toho-u.ac.jp (A. Ishigami).

[1] These authors contributed equally to this work.

0006-291X/$ - see front matter © 2008 Elsevier Inc. All rights reserved.
doi:10.1016/j.bbrc.2008.08.020

In 1991, we originally identified senescence marker protein-30 (SMP30) as a distinctive protein, the expression of which decreases in an androgen-independent manner with aging [11]. Moreover, we established SMP30/gluconolactonase (GNL) knockout (KO) mice, which cannot synthesize VC *in vivo*, because SMP30 is an alternative name for GNL, a factor in the VC biosynthetic pathway [12,13]. Our recent study revealed that the SMP30/GNL knockout (KO) mouse develops scurvy when fed a VC-deficient diet [12]. Moreover, oxidative stress increases in brains from SMP30/GNL KO mice, without influencing the status of other anti-oxidant enzymes such as superoxide dismutase, glutathione peroxidase, and catalase [14]. Thus, the SMP30/GNL KO mouse is a powerful tool for investigating the mechanism used by anti-oxidant agents to scavenge ROS exclusively without affecting other anti-oxidant enzymes.

In this study, we found that hydrogen-rich pure water scavenges superoxide in the brain slices from VC-depleted SMP30/GNL KO mice. The real-time biography superoxide system we used indicated that hydrogen acts as an anti-oxidant that specifically eliminates superoxide in the brain *in vivo*.

Materials and methods

Hydrogen-rich pure water. Pure water was produced by the following processes: passage through (1) a reverse osmosis/ultrafiltration unit, (2) an ion-exchange resin, and (3) an ultrafiltration membrane (pure water: pH 6.9 ± 0.05; electric conductivity 0.7 ± 0.2 μS/cm). Hydrogen-rich pure water then resulted from dissolving hydrogen gas directly into pure water and had the following physical properties: pH 6.7 ± 0.1, low electric conductivity (0.9 ± 0.2 μS/cm), high content of dissolved hydrogen (1.2 ± 0.1 mg/L), low content of dissolved oxygen (0.8 ± 0.2 mg/L), and an extremely negative redox potential (−600 ± 20 mV). To prevent the loss of hydrogen, the hydrogen-rich pure water was sealed in 300 mL aluminum pouches and stored at room temperature.

SMP30/GNL KO mice. SMP30/GNL KO mice were generated with the gene targeting technique described previously [13]. Female KO (*SMP30/GNL*$^{-/-}$) mice were mated with male KO (*SMP30/GNL*$^{Y/-}$) mice to produce all male and female KO mice. Genotypes of SMP30/GNL KO mice were determined as described previously [13]. SMP30/GNL KO mice were weaned at 30 days of age, at which time they were divided into groups with free access to either hydrogen-rich pure water (H_2), VC water (VC), or pure water (H_2O) for 33 days. The H_2 group drank hydrogen-rich pure water the VC group drank pure water containing VC (1.5 g/L) and 10 μM ethylenediaminetetraacetic acid (EDTA), whereas the H_2O group drank pure water without H_2 and VC. Glass water bottles containing H_2, VC, and H_2O were changed twice daily until the experiment ended. All mice were fed a VC-deficient diet (CL-2, CLEA Japan, Tokyo, Japan). Throughout the experiment, animals were maintained on a 12-h light/dark cycle in a controlled environment. All experimental procedures using laboratory animals were approved by the Animal Care and Use Committee of the Toho University and Tokyo Metropolitan Institute of Gerontology.

Preparation of brain tissue and VC measurement. Brains were rapidly removed from all mice and placed on a tissue cutter. Coronal slices cut 300 μm thick were transferred into ice-cold Krebs–Ringer solution (124 mM NaCl, 5 mM KCl, 2 mM $CaCl_2$, 1 mM $MgCl_2$, 1.2 mM KH_2PO_4, 26 mM $NaHCO_3$ and 10 mM glucose) equilibrated with 95% O_2/5% CO_2. For VC measurement, brain slices were homogenized in 10 mM Tris–HCl (pH 8.0) containing 1 mM PMSF by using glass-teflon homogenizer and centrifuged at 21,000g for 30 min at 4 °C. The supernatants obtained were immediately mixed with 5% metaphosphate and kept at −80 °C until use. Samples were treated with 0.1% dithiothreitol to reduce dehydroascorbic acid to ascorbic acid and analyzed by HPLC using an Atlantis dC18 5 μm column (4.6 × 150 mm, Nihon Waters, Tokyo, Japan). The mobile phase was 50 mM phosphate buffer (pH 2.8), 0.2 g/L EDTA, 2% methanol at a flow rate of 1.3 mL/min, and electrical signals were recorded by using an electrochemical detector with a glassy carbon electrode at +0.6 V [16,17]. Total VC in this preparation of brain tissue was measured by using a high-performance liquid chromatography (HPLC)-electrochemical detection method as described previously [15].

Dynamic chemiluminescence image of superoxide during hypoxia-reoxygenation in brain slices by real-time biography. To estimate the dynamic changes of superoxide radical formation during hypoxia-reoxygenation, we previously developed a real-time biography imaging system [18,19]. Here, we determined superoxide radical formation by chemiluminescence emission distribution imaging, for which the intact brain slices were pre-incubated in a chamber filled with oxygenated Krebs–Ringer solution with 2 mM *N,N'*-dimethyl-9,9'-biacridinium dinitrate (Lucigenin) (Sigma, St. Louis, MO, USA) for 45 min at 34 °C. After a 45 min pre-incubation, the brain slices were incubated for an additional 120 min in the same oxygenated environment (95% O_2/5% CO_2) in the imaging chamber at 34 °C. Then the conditions were made hypoxic (95% N_2/5% CO_2) for 15 min, returned to an oxygenated environment, and incubated again for up to 120 min. Images of brain slices were acquired every 15 min during the intervals of oxygenation, hypoxia, and then reoxygenatation for up to 255 min (17 frames). Image brightness was represented by the same scale in all frames.

Statistical analysis. Results are expressed as means ± SEM. The probability of statistical differences between experimental groups was determined by Student's *t*-test or ANOVA as appropriate. For one- and two-way ANOVAs, we used KaleidaGraph software (Synergy Software, Reading, PA, USA). Statistical differences were considered significant at $p < 0.05$.

Results

Effect of hydrogen-rich pure water on body weight

SMP30/GNL KO mice were divided into three groups, mice fed hydrogen-rich pure water (H_2), VC water (VC), or pure water (H_2O) after weaning at 30 days of age. To investigate the effect of H_2, VC, or H_2O administration on growth, we compared body weight changes (Fig. 1). All three groups of SMP30/GNL KO mice gained the same amount of weight throughout the experiment. That is, the body weights of H_2, VC, and H_2O administration groups at 63 days of age were 26.1 ± 0.5, 25.0 ± 1.1, and 24.9 ± 0.9 g, respectively.

Total vitamin C levels in the brain after ingestion of hydrogen-rich pure water

Next, we determined the quantity of total VC in the brains of SMP30/GNL KO mice fed H_2, VC, or H_2O, until they reached 63 days of age. The brains from H_2 and H_2O administration groups had <6% of the VC values obtained for SMP30/GNL KO recipients of VC (Fig. 2). Total VC level in brain slices from H_2, VC, and H_2O administration groups were 0.3 ± 0.1, 5.5 ± 0.4, and 0.3 ± 0.1 μg/mg protein, respectively.

Superoxide formation during hypoxia-reoxygenation in a model of the living brain

To ascertain whether hydrogen-rich pure water protects the brain from ROS generation, we measured superoxide formation during hypoxia-reoxygenation treatment with a real-time

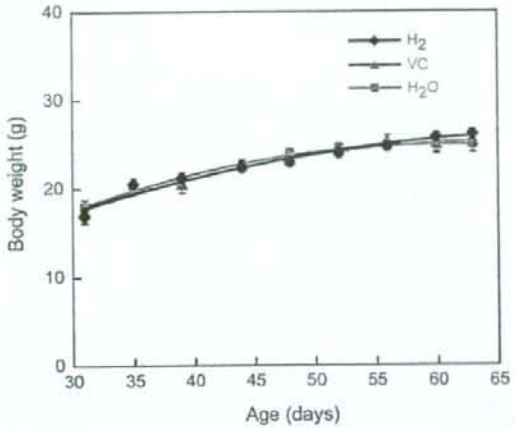

Fig. 1. Body weight changes of SMP30/GNL KO mice given either H_2, VC, or H_2O. SMP30/GNL KO mice weaned at 30 days of age were divided into three groups: recipients of either hydrogen-rich pure water (H_2), VC water (VC) or pure water (H_2O). Their body weights were measured, and the mean changes were plotted until the animals were 63 days of age. Values are expressed as a means ± SEM of 10 animals.

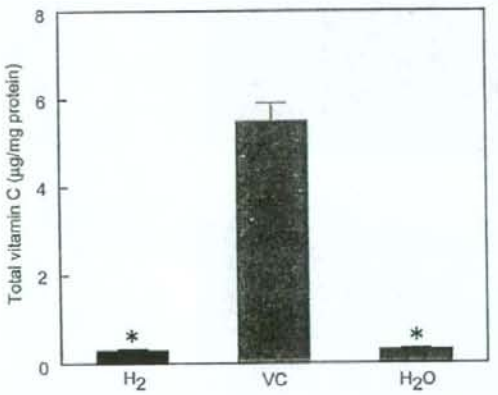

Fig. 2. VC levels in brains from the H_2, VC, and H_2O administration groups of SMP30/GNL KO mice. After weaning at 30 days, mice were grouped by those given free access to H_2, VC, or H_2O for 33 days. Glass water bottles containing H_2, VC, and H_2O were change twice daily until the experiment ended. Values are expressed as a means ± SEM of five animals. $^{*}p < 0.01$ as compared to the VC group.

biography imaging system using Lucigenin as chemiluminescence probe in brain tissues. Chemiluminescence emission images were obtained every 15 min from up the start of incubation until 255 min afterward, including the periods of oxygenation, hypoxia, and then reoxygenation. The time course of superoxide formation in the brain slices from H_2, VC, and H_2O administration groups of SMP30/GNL KO mice are shown in Fig. 3A. Superoxide formation was markedly decreased during the hypoxic condition (95% N_2/5% CO_2) and then increased during the oxygenated state lasting for 120 min. Superoxide formation in all three groups reached a maximum after 30 min of hypoxia, then gradually decreased and returned to the basal level. Superoxide formation at the maximal time of reoxygenation in H_2, VC, and H_2O administration groups was 7.45 ± 0.45, 5.36 ± 0.35, and 9.95 ± 0.74 counts/pixel for each 15 min reading, respectively. Superoxide formation during reoxygenation was calculated as an average over the 135–180 min time period (Fig. 3B). The H_2- and H_2O-only groups formed 1.9- and 1.4-fold higher levels of superoxide than the VC group did under the reoxygenation condition, respectively (Fig. 3B). Moreover, superoxide formation in the group given H_2 was a significant 27.2% lower than that in the H_2O administration group. A typical image of chemiluminescence in brain slices at basal, hypoxic, and reoxygenated conditions appear in Fig. 4. Superoxide formation was distributed heterogeneously throughout the brain regions and did not change significantly during hypoxia-reoxygenation treatment.

Discussion

In this study, we demonstrated that the administration of hydrogen-rich pure water created a pronounced decrease of superoxide formation in brain slices. These brain tissues came from VC-negative SMP30/GNL KO mice and were examined during hypoxia-reoxygenation treatment by using a real-time biographic system in which Lucigenin functioned as a chemiluminescence probe that detects superoxide. This outcome reflects a decrease of ROS generation in brain slices during ischemia and coincides with the report of Ohsawa et al. [9] indicating that hydrogen acts as a therapeutic anti-oxidant by selectively reducing ·OH. During ischemia, massive ATP consumption leads to accumulation of the urine catabolites hypoxanthine and xanthine, which upon subsequent reperfusion and influx of oxygen are metabolized by xanthine oxidase to produce enormous amounts of superoxide and ·OH [20]. We showed here that mice fed hydrogen-rich pure water formed 27.2% less superoxide when reoxygenated after an interval of hypoxia than mice fed pure water alone (Fig. 3). We speculate that the mechanism of this decrease in superoxide is the ability of hydrogen to reduce both ·OH and superoxide under specific conditions such as ischemia and reperfusion *in vivo*. Underlying this speculation is the fact that hydrogen can readily permeate the cell membrane and protect DNA from damage by ROS thereby influencing gene transcription [8,9]. An alternative possibility is that hydrogen permeates mitochondria and directly reduces the production of superoxide.

Recently we reported that superoxide-dependent chemiluminescent intensity in brain tissues from senescence accelerated mice (SAM) of the C57/BL6 strain, Wister rats, and pigeons clearly increased in an age-dependent manner [19]. The rate of this age-related increase in superoxide-dependent chemiluminescence was inversely related to the maximal lifespan of these animals; however, the activity of superoxide dismutase (SOD) in the brain was unchanged during the aging process. These findings strongly suggest that the reactive oxygen may be a signal that determines the aging process. Here, we used SMP30/GNL KO mice, which cannot synthesize VC *in vivo* [12], as a model of aging and oxidative stress and found that, in the absence of VC supplementation, superoxide generation in the brain slices increased during hypoxia-reoxygenation treatment (Figs. 2 and 3). VC is well known as a strong anti-oxidant that removes superoxide *in vitro* [21–24]; however, there is less evidence to prove that this effect actually occurs *in vivo*.

In our hands, reactive oxygen-dependent chemiluminescence was visible in a heterogeneous distribution throughout the brain (Fig. 4), although the intensity was greater in white matter than in gray matter. This heterogeneity did not significantly change during oxygenation and hypoxia-reoxygenation. However, since Okabe et al. [25] found less SOD activity in white matter than gray matter by histochemical localization analysis, the greater chemiluminescent intensity we noted in white matter could be explained by the latter's weaker SOD activity.

Subsequently, Fukuda et al. reported that inhalation of hydrogen gas suppressed hepatic injury caused by ischemia–reperfusion